ARCTIC SEA ICE AND ATMOSPHERIC CIRCULATION ANOMALIES SINCE 1954

by

Victoria C. Slonosky

A thesis submitted to the Faculty of Graduate Studies and Research in partial fulfilment of the requirements for the degree of

MASTER OF SCIENCE

Department of Atmospheric and Oceanic Sciences
McGill University
Montréal, Québec

0-612-37305-3

ABSTRACT

The relationship between Arctic sea ice concentration anomalies, particularly those associated with the "Great Salinity Anomaly" of 1968-1982, and atmospheric circulation anomalies is investigated. Empirical orthogonal function (EOF) analyses are performed on winter and summer sea ice concentrations, sea-level pressure, 500 hPa heights and 850 hPa temperatures: these data cover the Northern Hemisphere north of 45°N during the post-World War II era. Spatial maps of temporal correlation coefficients between EOF 1 of winter sea ice concentration and the atmospheric anomaly fields are calculated. Significant correlations (at 95 and 99% levels) were found to exist between EOF 1 of winter sea ice and the atmospheric anomaly fields at zero lag, and with ice leading by one and one-and-a-half years, and ice lagging by one year. The main emphasis of the thesis is to identify connections between Arctic sea ice and atmospheric circulation anomalies at interannual timescales.

RÉSUMÉ

Cette étude tente d'établir s'il existe une relation entre les anomalies de la glace océanique arctique, en particulier celles reliées à la grande anomalie de salinité de 1968-1982 et les anomalies de la circulation atmospherique. Des analyses en terme de fonctions empiriques orthogonales (EOF) sont effectuées sur des données saionnières d'hiver et d'été de glace océanique, de pression au niveau de la mer, d'hauteur géopotientielle à 500 hPa, et de témperature à 850 hPa: ces données englobent l'hémisphère Nord à partir de 45°N pour la periode depuis la deuxième guerre mondiale. Des cartes des corrélations temporelles entre la première EOF de la glace océanique hivernales et les anomalies atmosphériques sont calculées. Des corrélations significatives de plus de 95% existent entre la couverture de glace et les conditions atmosphériques pour la même année, l'année précédente et l'année suivante. Ce mémoire met l'accent sur l'identification des rapports entre la glace océanique et les anomalies de circulation atmosphériques à une échelle de temps interannuelle.

ACKNOWLEDGMENTS

I am very grateful for the advice and support of my supervisors, Dr. J. Derome and Dr. L.A. Mysak, to Bill Chapman, for his help with the sea ice concentration data, and to Dennis Joseph for his assistance with the sea level pressure data. I would also like to thank Dinh Hai Tran, Marc Klasa, Hai Lin, Halldor Bjornsson, and Gary Kennedy for their patient computer and programming help, and Bruno Tremblay for his critical advice. Last but not least, I thank my parents for their encouragement and understanding.

This research was undertaken while the author was financially supported by a scholarship from le Fonds FCAR (Fonds pour la formation des chercheurs et l'aide à la recherche). This work was also supported in part by research grants awarded to Dr. J. Derome and Dr. L.A. Mysak by NSERC and the Atmospheric Environment Service.

TABLE OF CONTENTS

1. INTRODUCTION

The interaction between sea ice concentration and atmospheric circulation anomalies is an important factor in the generation and maintenance of high latitude climate variability. It is widely believed that patterns of sea ice cover are determined by atmospheric wind forcing, since sea ice drift and upper ocean currents are mainly wind driven (Walsh, 1978; Walsh and Chapman, 1990a). The presence of sea ice, on the other hand, can influence the atmospheric circulation mainly through its effect on air-sea heat exchange, and to a lesser extent by affecting moisture and momentum exchange processes between the ocean and atmosphere (Agnew, 1993). Since the atmospheric circulation is itself a function of diabatic heating (Walsh and Johnson 1979b), interactions between sea ice and atmospheric circulation have a large influence on mid and high latitude climatic variability.

The goal of this thesis is to determine what relationship, if any, exists between Arctic sea ice concentration and atmospheric circulation anomalies north of 45°N on seasonal and longer timescales. Particular emphasis is placed on the ice anomalies that accompanied the "Great Salinity Anomaly" in the northern North Atlantic from 1968-1982. By decomposing data fields using Empirical Orthogonal Functions and correlating patterns of ice variability associated with the "Great Salinity Anomaly" with atmospheric anomaly fields, some connections between sea ice and atmospheric anomalies become apparent. Interactions on interannual to decadal timescales are investigated in this thesis as much of the variability in the sea ice concentration occurs on these timescales (Fang and Wallace, 1994; Mysak et al., 1990; Mysak and Power 1992; Deser and Blackmon

1993).

1.1 The Great Salinity Anomaly

The Great Salinity Anomaly (GSA) was a period of low upper ocean salinities and sea surface temperatures (SSTs) which occurred in the Greenland-Iceland Sea and the northern North Atlantic from the mid 1960s to the early 1980s (Dickson et al., 1975; 1988), and may be the second largest signal in the ocean climate signal after the El Niño (Walsh and Chapman, 1990b). This negative salinity anomaly was first noticed in the Greenland-Iceland Sea just north of Iceland in the mid to late 1960s, and was accompanied in these locations by large sea ice extents (Mysak and Manak, 1989; Mysak et al., 1990). It travelled cyclonically around the sub-polar gyre, reaching the coast of Labrador in 1971, and was then advected eastward to northwestern Europe a few years later (Figure 1.1). The anomaly eventually returned, although in a weakened state, close to the area of its origin in the Greenland Sea 13 or 14 years after its first appearance.

Minimum sea surface temperatures, over 2°C below normal, were observed north of Iceland in 1967, while minimum salinities of over 0.5 practical salinity units (psu) below normal and maximum sea ice extent occurred in the Greenland-Iceland Sea a year later (Mysak et al., 1990, Marsden et al., 1991). Low temperatures (up to 4°C below normal) and salinities (1 psu below average) were next observed off the coast of western Greenland from 1969-1971. The absolute salinity minimum in this region of 1.9 psu below normal in 1969 represents a departure of over three standard deviations from the 23-year average (Dickson et al., 1988). The negative salinity anomaly subsequently propagated around the Labrador Sea, following the west Greenland current northward up the west coast of Greenland to the head of Baffin Bay, then returning southward with the Labrador current and becoming detectable off the coast of Labrador in 1971. Salinity and temperature anomalies measured east of Newfoundland from 1971-1973 were of the same magnitude and duration as those measured two years earlier off western Greenland. It is thought that local freshening due to runoff could have caused the anomaly to persist in the region for some time (Dickson et al., 1988).

The temperature and salinity anomalies were then advected eastward by the subpolar gyre. Evidence from some fragmentary records suggests that the GSA was in the mid-Atlantic region from about January 1974 until June 1975, although it appears to have been considerably weakened (Dickson et al., 1988). The GSA was observed in the Faroe-Shetland Channel in 1976, and in the Norwegian Sea in 1977. Low values of temperature and salinity were observed off the coast of northern Scandinavia in 1978, and low salinities near Spitsbergen in 1979. The anomaly would then have been advected by the West Spitsbergen Current, with a part of the anomalously fresh water passing northwards into the Barents Sea and eventually to the Laptev Sea, and a part returning to the Greenland Sea. Low salinities were observed west of Fram Strait in the summer of 1982, which would be the most reasonable assumed date of the return of the anomaly to the Greenland Sea (Dickson et al., 1988).

Positive sea ice extent anomalies were prevalent in the Greenland Sea during the 1960s, prior to and coincident with the GSA. The positive sea ice anomaly in the Greenland Sea was well established by 1966, and reached a maximum in 1968. Severe ice conditions existed along the entire east coast of Greenland from 1970 until 1972, and a large positive ice anomaly was noted in the Labrador Sea during the same period (Mysak and Manak, 1989). There were also very high ice concentrations around Iceland during the peak years of the 1968 GSA event, as Koch ice index values were high from 1965 to 1973 (Mysak et al., 1990). It would appear that the salinity anomaly caused the ice anomaly in the Labrador Sea, as the ice peak of 1972 in that region was preceded by a negative salinity anomaly some 16 months earlier (Mysak et al., 1990). The ice anomaly subsequently strengthened the salinity anomaly by contributing fresh water to the region through ice melt in summer.

The GSA first appeared in the Greenland-Iceland Sea in 1964 (Dickson et al., 1988); sea-ice formation was enhanced during the winter of 1965 (Mysak and Manak, 1989). Ice and salinity anomalies, once formed, can perpetuate themselves for some time, as fresh water tends not to sink or mix vertically, but instead freezes (Marsden et al., 1991; Lazier 1980). When this ice melts, either as the seasons change or as it is advected into warmer latitudes, a surface layer of cold, fresh, low density water is created which prevents vertical mixing and perpetuates the anomaly. This suppression of vertical mixing inhibits deep water formation, and can have a profound effect on the thermohaline circulation. It is probably because of this lack of convective mixing that the GSA was traceable as a coherent signal for over 10 years.

Sea surface temperature anomalies are also concurrent with the Great Salinity Anomaly. Low sea surface and upper ocean temperature observations accompanied the GSA as it propagated around the northern North Atlantic (for more information, see

Dickson et al, 1988). These low temperatures can be related to the presence of sea ice cooling the surrounding water, and to the low temperature of meltwater produced by sea ice. Again, these anomalies tended to persist as there was little convective mixing.

1.2 Origin of the GSA

Several researchers ascribe the formation or accumulation of the large sea ice and salinity anomalies in the Greenland-Iceland Sea to atmospheric forcing (Dickson et al, 1988, Walsh and Chapman 1990b, Serreze et al., 1992). Prior to the 1968 GSA event, the Icelandic Low weakened and a high pressure ridge was established in the sea level pressure anomaly field over the northern North Atlantic and Greenland region, which increased in strength from 1956 until 1970 (Figure 1.2). As noted by Dickson et al. (1975), this high pressure anomaly was responsible for bringing unusual amounts of cold polar air to northern Europe and warmer southern air into the Labrador and Baffin Bay region by increasing the amount of anticyclonic circulation over the North Atlantic. This anomalous ridge collapsed dramatically in 1970 and was replaced by an intensified Icelandic-Greenland Low. During the years of the high pressure anomaly (Figure 1.2b) colder and fresher polar water entered the Greenland Sea from the Arctic Ocean, causing an anomalously large amount of sea ice to be formed in and/or advected into this sea (Dickson et al, 1975; Häkkinen, 1993). From 1964 to 1971 the east Icelandic current became a polar current, transporting and preserving drift ice as well as transporting a large amount of relatively fresh Arctic water into the North Atlantic region; it had previously (i.e., from 1948-1963) been an ice free current (Dickson et al., 1975). The weakened Icelandic Low of the 1960s reduced northward heat transport, resulting in increased ice formation in the Arctic. The anomalous northerlies of the east coast of Greenland led in turn to the subsequent southward transport of Arctic sea ice, resulting in heavy ice conditions in the Greenland Sea (Power and Mysak, 1992).

In their 1990b paper, Walsh and Chapman postulated that the atmospheric circulation anomalies over the northern North Atlantic and unusual atmospheric circulation over the Arctic combined to produce the circumstances which led to the GSA. As well as the higher than normal sea level pressures in the northern North Atlantic and Greenland regions, they found that there was an anomalous low pressure centre over the Arctic Ocean (centred over the Kara Sea) for the period from April 1967 to March 1968 (Figure 1.3). Serreze et al. (1992) further analyzed the sea level pressure field over the Arctic and discovered that while the frequency of cyclones remained fairly constant during the 1960s, the frequency of anticyclones increased over Arctic land areas and decreased over the Arctic Ocean during the period from 1967 to 1970. This pressure distribution, combined with the northerly flow over the Greenland Sea, enhanced the transport of the thick, multi-year ice found north of Greenland and Ellesmere Island directly through the Fram Strait. According to Walsh and Chapman (1990b), the GSA occurred subsequent to an "atmospherically unique" period when the high latitude atmospheric circulation was in a highly anomalous state, leading to increased ice export through the Fram Strait.

Mysak et al. (1990) proposed that large sea-ice concentrations in the Greenland Sea are caused in part by higher than normal river runoff from North America into the western Arctic Ocean; it was established that a statistically significant lag of 3 to 5 years existed between North American runoff into the Arctic Ocean and sea-ice concentration anomalies in the Greenland Sea (Mysak and Power, 1992). Bradley and England (1978) noted a "climatic jump" between 1963 and 1964, when there was a marked, step-like decrease in summer Arctic temperature and increase in precipitation which may have caused the increase in Arctic runoff. The large amounts of fresh water runoff into the Arctic Ocean would have increased the stability of the water, preventing overturning and enhancing ice formation. The ice anomaly would then have propagated to the north of Greenland via the Beaufort gyre, adding to the ice convergence in that area caused by the anomalous northerly winds. The extensive Arctic ice would then have been exported out of the Arctic by the Transpolar Drift Stream, eventually entering into the Greenland-Iceland Sea where the GSA was first observed.

1.3 Influence of the GSA on the atmosphere

There are several ways in which the GSA may have influenced the atmospheric circulation. Sea ice has a high, albeit somewhat variable, albedo of about 80%, affecting the radiation budget of its surroundings (Power and Mysak, 1992). The presence of extensive sea ice cover also reduces the sensible heat loss from the ocean to the atmosphere, and suppresses evaporation from the sea surface and hence the formation of clouds in the lower atmosphere (Power and Mysak, 1992). In their feedback loop, Mysak and Power (1992) suggest that the large ice and salinity anomalies which suppressed convective overturning and deep water formation in the northern North Atlantic created negative SST anomalies, which decreased sea-to-air heat fluxes and thus cyclogenesis over the Irminger Basin. This decreased cyclogenesis would have created air masses in that region which were drier and colder than normal, and may be related to the increased frequency of anticyclones over the Canadian Arctic Archipelago noted by Serreze et al. (1992). It would therefore be expected that the GSA would have created cold pools of air over the North Atlantic, increased anticyclogenesis, and/or decreased cyclogenesis.

The main questions that will be addressed in this thesis are 1) what is the influence of the sea ice on the atmosphere, and 2) what is the nature of the interactions between sea ice concentration anomalies and atmospheric circulation patterns? A description of the data analyzed, namely sea level pressure, 850 hPa temperatures, 500 hPa geopotential heights and sea ice concentration is given in Chapter 2, while Chapter 3 consists of a summary of the analytical techniques used in this thesis; anomaly (observation - mean) calculations, Empirical Orthogonal Function (EOF) analysis and equations for the calculation of cross-correlations and significance levels. EOF decompositions are calculated for every field, and the correlation coefficients between the time series of the leading EOF of winter sea ice and the atmospheric anomaly fields are computed in a manner similar to techniques used by Fang and Wallace (1993). Maps of the difference fields between the state of the atmospheric circulation and sea ice cover in the 1950s, 1960s and 1970s are presented in Chapter 4, along with four-year mean anomaly maps of all the variables, starting in 1963 and ending in 1974. The results of the EOF analyses are also presented in Chapter 4. Chapter 5 consists chiefly of the presentation and discussion of the correlation maps. Finally, a summary of the main conclusions is given in Chapter 6.

2. DATA

Two sets of data have been analyzed: atmospheric data, which is comprised of sea-level pressure (SLP), 850 hPa temperature (850 T), and 500 hPa geopotential heights (500 Z), and sea ice concentration data (IC).

2.1 Atmospheric data

The 850 hPa temperatures and 500 hPa geopotential heights were taken from the U.S. National Meterological Center (NMC) archives. Twice daily data for 500 hPa geopotential heights were available from 1947 to 1988 from the NMC CD-ROM, while twice daily 850 hPa temperatures were available only for 1963 to 1988. NMC data for 500 Z and 850 T from 1989 to 1994 were obtained from a set of NMC international exchange format magnetic tapes. The data were usually based on NMC final analyses, which include information received up to 10 hours after observation time. If the final analyses were not available, the operational analyses, which include information received up to 3 hours after observation time, were used instead. The NMC CD-ROM contains monthly means which are calculated from twice daily data, whereas the tapes contain only the twice daily data.

The SLP data for the entire period (1947-1994) were obtained from the U.S. National Centre for Atmospheric Research (NCAR) anonymous ftp site, which is operated by the University Corporation for Atmospheric Research and sponsored by the U.S. National Science Foundation. This data set was used as SLP data from 1989 to 1994 were not available on the international exchange format magnetic tapes. The SLP monthly means were calculated from twice daily NMC final analyses. All atmospheric data were stored on the NMC octagonal grid, an equally spaced grid based on a polar stereographic projection true at 60°N, with data extending down to 20°N (Jenne, 1970).

Although data in the Arctic region tend to be sparse, the inclusion of reports from drifting ice stations, beginning in 1952, greatly increased the reliability of Arctic data (Serreze, 1995; Walsh, 1978). Data from the Arctic buoy program in the 1970s further increased the quality of the high latitude analyses.

Once monthly means had been calculated when necessary from the twice daily data, annual winter and summer means were determined for each variable; the values for the winter means are calculated from the monthly mean for the December of the preceding year, and the January and February monthly means of the given year. The summer mean values are calculated from the monthly means for June, July and August. No data were available for August 1994, so the summer mean for 1994 is composed of the means for June and July only. Winter and summer climatologies and variances were calculated for each atmospheric field, and winter and summer anomaly data sets were calculated by subtracting the seasonal climatology from the seasonal mean for each year. Winter and summer climatology maps for each atmospheric variable are presented in Figures 2.1, 2.2, and 2.3.

Pressure and temperature data over areas of high elevations, such as the Rockies, the Himalayas and Greenland, where the sea level and 850 hPa surfaces do not exist (they would be beneath the land surface), produced spuriously high temporal variances (not shown). As it was not known what methods were used to estimate temperatures and sea level pressures over these areas, and as these methods produced very high anomalies of both signs at various periods in the record, filters based on elevation, in the form

$$f = 1 - \frac{elevation}{maximum\ elevation}$$

where the maximum elevation is the highest elevation in the domain (i.e., north of 45°N), were applied to the SLP and 850 T data. Outliers in the data set were also identified by generating maps of high order moments of the anomaly fields to determine when and where individual points of suspiciously high variance were situated: the values of the anomalies at these points were then reduced to one third their original value, as it was felt that this produced the most reasonable results, reducing the influence of spurious data while retaining some of the original variance. Filtered variance maps (not shown) show maxima over the North Atlantic, Greenland and central Arctic for winter SLP and 500 Z, while winter 850 T maxima in variance occur over central Canada and Greenland. A maximum occurs over the central Arctic in the summer SLP variance map, and over the North Atlantic in summer 500 Z. The summer 850 T variance field is fairly flat.

2.2 Sea ice data

The sea ice concentration data used were the monthly Arctic sea ice concentration grids provided by Dr. J. Walsh and Mr. W. Chapman from the University of Illinois. Ice concentration maps are available from 1901 to 1990, although the data before 1954 was discarded as its reliability is questionable and its inclusion produced irregularities in the data analysis. An essentially continuous record in the North American Arctic began in 1953 (Walsh and Johnson, 1979b). The data set contains monthly values of sea ice concentration representing the coverage at the end of a given month. The sea ice concentrations are stored on an equal area grid, and each grid box has a dimension of 110.8 km by 110.8 km. Concentration values are reported in tenths, ranging from 0/10, (no sea ice was reported in the grid area at the end of a particular month) to 10/10 (the grid area was completely ice covered at the end of that month).

Although the heaviest ice concentrations are found in early March and the lightest in September, the months of December, January, February and June, July, August were used in calculating the ice winter and summer composites, respectively. This means that the "winter" ice season does not contain the month with the heaviest concentrations, nor "summer" the month with the lightest concentrations. Note that there is an implicit half month lag between the sea ice concentrations and the atmospheric monthly means, as the former are composed of end of the month values.

The six main sources of sea ice data that were used by Walsh and Chapman to compile this data set were from the Danish Meteorological Institute, the Japan Meteorological agency, the U.S. Naval Oceanographic Office, the Kelly ice extent grids, Walsh and Johnson/U.S. Navy-NOAA Joint Ice Centre, and the U.S. Navy-NOAA Joint Ice Centre Climatology. Some temporal extensions of the Kelly grids based on autocorrelations were also used. A nearest neighbour interpolation scheme was used to transform the data from Walsh and Chapman's equal area ice concentration grid (IC_{WC}) to the NMC polar stereographic grid (IC_{NMC}). The latitude and longitude of each grid point were known for both grids, and so for each NMC grid point, a weighted average based on inverse distance was calculated from those points in the Walsh and Chapman sea ice grid which were no more than 200 km away from the NMC grid point (W. Chapman, personal communication 1996):

$$IC_{NMC} = \frac{\sum \frac{1}{r_i^2} IC_{WC}}{\sum \frac{1}{r_i^2}}, \qquad r_i < 200\ km,$$

where

$r_i = r_e\, \gamma$;

r_e = radius of earth,

$$\gamma = \arccos[X_{NMC}X_{WC}+Y_{NMC}Y_{WC}+Z_{NMC}Z_{WC}],$$

$X = \cos\varphi \cos\theta$,

$Y = \cos\varphi \sin\theta$,

$Z = \sin\varphi$

θ = longitude, and

φ = latitude.

(Distances were calculated as arclengths along a great circle, and grid points over land were omitted, so as to not unduly influence the weighted average).

Winter and summer sea ice concentration climatologies are presented in Figure 2.4. Maxima in the winter variance map (not shown) exist over the Greenland Sea and the central Arctic region, while maxima in the summer variance map (not shown) occur in the Mackenzie delta and the Gulf of Ob.

3. METHODS OF ANALYSIS

Climatologies (time means) and anomaly fields (observation - climatology) were calculated for each variable. An EOF analysis was performed on the sea ice concentration anomaly data and on the atmospheric anomaly data north of 45°N only, and the results are presented in Chapter 4. It was decided to use only data north of 45°N in order to capture the mid to high latitude atmospheric forcings for and responses to the Arctic sea ice concentrations. It was thought that if data from the entire NMC grid down to 20°N were used, low latitude variability such as that associated with the El Niño-Southern Oscillation may overwhelm other climate signals and obscure high latitude variability.

It was found that the first EOF of winter sea ice concentration best described the GSA (see Chapter 4), and so spatial maps of the temporal correlation between the atmospheric anomaly fields and the negative of the time series of EOF 1 of winter sea ice concentration were calculated. These maps are presented in Chapter 5.

3.1 Empirical Orthogonal Functions

An EOF analysis is a method of reducing a data set into a series of orthogonal basis vectors. The covariance matrix of a spatial and temporal array is computed, and a set of eigenvectors is obtained from this covariance matrix such that the basis chosen best represents the variance of the original data. That is to say, the sum of squares of the projection of the observations onto the eigenvectors is maximized. The eigenvectors are ordered such that the leading EOF (the first eigenvector) explains the most variance contained in the data set, and the second EOF the next most variance, and so on, while the actual proportion of the variance explained by a given EOF is its eigenvalue. The EOFs are sometimes described as modes of variability, and the number of EOFs obtained is equal to the dimension of the covariance matrix. The EOF consists of both a spatial pattern and a time series describing changes in the amplitude of that spatial pattern over the length of the record. This time series is obtained by projecting the original data matrix onto the eigenvectors.

To calculate the covariance matrix the spatial data are ordered as the columns in an array: a two-dimensional array is formed with each column containing all the spatial data points (the map) at one time:

$$D = \begin{vmatrix} d_{1,1} & \cdots & d_{1,N} \\ \cdots & & \cdots \\ d_{M,1} & \cdots & d_{M,N} \end{vmatrix},$$

where N is the number of time points, $(d_{m,1},..,d_{m,N})$ is the time series of each grid point, and M is the number of spatial grid points.

The covariance matrix is proportional to the two dimensional data matrix D multiplied by its transpose:

$$C = \frac{1}{N} D\, D^{T}.$$

Since the object is to find a basis formed of mutually orthogonal vectors $\mathbf{e}_m$ (m=1,...,M) such that the sum of squares of the projection of all data vectors onto each basis vector **e** is maximized sequentially (i.e. the first basis vector describes the patterns which contain the most variance, the second vector describes the orthogonal and independent pattern which explains the next most variance, and so on), it is necessary to maximize the following expression (Peixoto and Oort, 1992):

$$\frac{1}{N}\sum_{n=1}^{N}[d_n \cdot e_m]^2 \quad for\ m=1,\ M.$$

Since the basis vectors are orthonormal,

$$e_m^{\,T}\ e_m=1,\quad e^{T}_{\ m}\ e_j=0,\quad j\neq m.$$

Thus, (Peixoto and Oort, 1992)

$$\frac{1}{N}\sum_{n=1}^{N}[d_n \cdot e_m]^2 = \frac{1}{N}[e_m^{\,T}\ D\ D^T\ e_m] = e_m^T\ C\ e_m,$$

Maximizing the expression $e_m^T C\ e_m$ subject to the constraint that the basis vectors e are orthonormal is an eigenvalue problem, and can be described as (Peixoto and Oort, 1992):

$$C\ e_m = \lambda\ e_m, \rightarrow (C-\lambda I)\ e_m = 0.$$

This is an algebraic equation of degree M in λ, with M solutions or eigenvalues $\lambda_1,\ldots\lambda_M$ which are real and positive, since C is symmetric and positive definite. The trace of C is invariant under basis transformations, and so is equal to the sum of the eigenvalues. Each eigenvalue therefore accounts for a certain fraction of the total explained variance, with the corresponding eigenvector containing the spatial pattern of the explained variance.

Since the eigenvectors form a basis, any data vector can be formed from a linear

Since the eigenvectors form a basis, any data vector can be formed from a linear combination of the eigenvectors:

$$\boldsymbol{d}_n = \sum_{m=1}^{M} a_{mn} \cdot \boldsymbol{e}_m.$$

The values of the coefficients a can be found by projecting the original data vectors $\mathbf{d}_n$ onto the basis vectors $\mathbf{e}_m$, so that $a_{mn} = \mathbf{e}_m{}^T\mathbf{d}_n$. The n coefficients a_m represent the time series of the coefficients of the eigenvector m, and the vectors formed by the m time series of a_n are also mutually orthonormal (Peixoto and Oort, 1992).

The EOF analyses were carried out on atmospheric and sea ice data in polar stereographic coordinates. When data collected on a spherical surface (the earth) are transformed into a two dimensional representation (as a map), there is some spatial distortion. A weighting factor was therefore applied prior to the EOF analysis to ensure that the value of all data points in the grid were representative of the area they covered. All values were multiplied by the square root of the inverse of the map scale factor:

$$\left(\frac{1 + \sin\phi}{1 + \sin 60^\circ}\right)^{\frac{1}{2}},$$

where φ is latitude. The square root of the correction factor was taken because the data points are multiplied by each other in the calculation of the covariance matrix.

3.2 Correlation coefficients

The sample correlation coefficient r is calculated as:

$$r = \frac{\sum_{n=1}^{N} X_i' Y_i'}{\sqrt{\sum_{n=1}^{N} (X_i')^2 \sum_{n=1}^{N} (Y_i')^2}}.$$

where the ' denotes departure from average.

For a fairly large sample size (N ≥ 10), a normal statistic Z for r can be approximated as (Medenhall et al, 1990):

$$Z = \frac{\frac{1}{2}\ln\left(\frac{1+r}{1-r}\right)}{\frac{1}{\sqrt{N-3}}}$$

for the null hypothesis that ρ, the true correlation coefficient, is zero. In order to have 95% confidence of rejection of the null hypothesis if $\rho \neq 0$ for a two-tailed test, the value of Z must be greater than or equal to 1.96 (2.57 for 99%). The value of the correlation coefficient r_{sig} corresponding to the Z threshold can therefore be calculated as:

$$r_{sig} = \frac{\exp\left(2 \cdot \frac{Z_{0.025}}{\sqrt{n-3}}\right) - 1}{1 - \exp\left(2 \cdot \frac{Z_{0.025}}{\sqrt{n-3}}\right)}.$$

Note that this number depends on the number of independent observations in the sample; the significance values for correlations with 850 T will be higher than the others because the data record is shorter. There is a certain amount of autocorrelation in the data fields, which is to say the fields are correlated with themselves at different time lags. At zero lag, the autocorrelation is 1, as any field is perfectly correlated with itself. If there were no autocorrelation and the data points for each field were independently and identically distributed (a key assumption for determining the significance levels from a normal distribution), the autocorrelation of a field with itself at any time lag which is *not* zero would be zero. However, the autocorrelation of the sea-ice concentration at a lag of 1 year is actually 0.6, which is significantly different from zero at the 95% confidence level. At a lag of 2 years the autocorrelation drops to 0.2, which is not significantly different from zero for the sea ice data. Therefore, in the above equation, the number of points N was initially divided by two, on the premise that data separated by two years or more are independent. The memory of the atmospheric fields is not as high as that of the sea-ice (Walsh and Johnson 1979a), and every second year of atmospheric data can also be considered independent. The areas of significant correlations are those where $r > r_{sig}$, and $r < -r_{sig}$.

Maps of the correlation coefficient between the time series of the atmospheric anomaly fields at each (spatial) grid point and the negative of the first EOF of winter sea ice concentration were calculated for different leads and lags. A negative lag time is defined here as an atmospheric lead, and a positive lag as an ice lead. A lag time of -1 year represents the correlation between the state of the atmosphere and the state of the ice one year later. When the correlations are interseasonal the lags are in fact increased by a half; thus the correlation between the winter ice of one year and the summer atmosphere of that same year has a lag of +1/2. The atmospheric time series was lagged with the sea ice concentration by up to +5 1/2 and -5 years (the data record was too short for many meaningful comparisons, especially with regard to the 850 hPa temperatures, beyond these time lags).

A Monte Carlo analysis for significance was then performed for each of the atmospheric variables, assuming zero lag. The time series of the first EOF of winter sea ice concentration was randomly reordered one thousand times, and correlation maps between the atmospheric anomaly time series and the randomized sea ice time series were calculated. The highest 25 and lowest 25 values for each grid point were discarded, and the twenty-sixth highest and twenty-sixth lowest values were then used as the 95% Monte Carlo significance levels for each grid point. The Monte Carlo technique is a method of calculating the probability of obtaining areas of random correlations in a field of spatially correlated values (Livezey and Chen, 1983). The significance levels obtained using the Monte Carlo technique tended to be near 0.34, with little spatial structure (i.e., all values tended to be between 0.32 and 0.37) for all three atmospheric fields. These values were much lower than those obtained using the above equation and dividing N by two, which started at 0.46 (0.53 for 850 T). It is felt that the probabilities of obtaining significant correlations by chance (the Monte Carlo results) were much lower than the significance levels previously calculated because the effect of temporal autocorrelation in the time series of EOF 1 of winter sea ice concentration had probably been overestimated by dividing N by two. Accordingly, new significance levels were calculated, again using the above equation but this time dividing N by only 1.5. These significance levels, starting at 0.4 for zero lag SLP and 500 Z (0.46 for 850 T) are still higher than the Monte Carlo significance levels obtained for spatially dependent data, and are the ones used in the correlation maps presented in the rest of this thesis.

A test described by Livezey and Chen (1983) as a precursor to the Monte Carlo analysis is a test for field significance assuming spatial independence. It is expected that individual points of significant correlation may occur randomly in a large sample.

Livezey and Chen (1983) have devised a test for field significance of (assumed) spatially independent data based on the binomial distribution. In order for a map of statistically significant areas of correlation to have field significance at the 95% level, more than a certain percentage (6.4%, or 32 grid points for the maps presented in this thesis) of the field must be significantly correlated. All correlation maps presented in this thesis have field significance at the 95% level assuming spatial independence, unless stated otherwise.

4. ANOMALY MAPS AND EOF RESULTS

In this chapter the state of circulation during the late 1950s and 1960s is first described. This period is analyzed as it was a time of highly anomalous atmospheric circulation over the Arctic and subarctic regions which is believed (Dickson et al., 1975, 1988, Walsh and Chapman 1990, Serreze et al., 1992) to have caused the Great Salinity Anomaly and associated ice anomalies in the late 1960s and early 1970s (see Chapter 1). The state of the atmosphere in the late 1960s and early 1970s is also examined in order to gain an understanding of the period after the initial formation of the GSA, when the ice and salinity anomalies were present in the northern North Atlantic. Finally, the results of the EOF analyses on the atmospheric variables (SLP, 850 T and 500 Z) and the sea ice concentration are presented.

4.1 Difference maps, 1954-1974

The nature of the atmospheric circulation during the late 1950s and 1960s was extremely unusual. Difference maps similar to those presented by Dickson et al. (1975) (see Chapter 1, Figure 1.2) were calculated for the entire polar region. All the maps presented in this section represent the earlier period subtracted from the later period (for example, the difference map for SLP 1956-1965/1966-1970 is the result of average SLP from 1956 to 1965 subtracted from average SLP from 1966 to 1970). The winter high pressure anomaly noted by Dickson et al. (1975) over Greenland and the Greenland Sea was also present in this analysis (Figure 4.1a), but extended over the Barents Sea and northern Russia as well, where average winter pressures in the late 1960s were up to 6 hPa higher than for the period 1956-1965. Over western Europe, on the other hand, pressures during the late 1960s were up to 3 hPa lower than 1956-1965 average values (Figure 4.1a). The difference map for 500 Z for the same period (Figure 4.1b) has a similar pattern, although the western high pressure difference cell is centred over the

Labrador Basin, farther south than the SLP centre. The difference maps for 1963-1970 and 1971-1974 (Figure 4.2) show large changes in the state of the atmosphere between the 1960s and the early 1970s. Mean sea level pressures (Figure 4.2a) over the northern North Atlantic and northern Russia were between 3 and 8 hPa higher during the period from 1963-1970 than they were from 1971-1974. The 500 Z difference field for the same period (Figure 4.2b) shows three distinct cells: an area where heights were higher in the 1960s centred over southern Greenland, an area where they were lower in the 1960s centred over the Baltic Sea, and a second area where heights were higher in the 1960s centred over western Russia. The patterns of height differences suggest the 500 hPa circulation during both the 1960s and the early 1970s had a strong meridional component, a suggestion which will be confirmed in the next section. Difference maps for the period 1967-1970 versus 1971-1974 (Figure 4.3) are qualitatively very similar to those in Figure 4.2, but with more pronounced features (i.e. larger differences). The GSA peaked during the 1967-1970 period.

The difference maps for winter 850 T show that the temperatures are higher during the 1960s than the 1970s over northern Canada (Figures 4.2c, 4.3c), while they are lower during the 1960s than the 1970s over the eastern Atlantic, western Europe and the central polar region (note that there are no temperature difference maps for the periods 1956-1965 and 1966-1970 as the temperature record only started in 1963; see Chapter 2).

In all the maps of SLP and 850 T, there are strong gradients near and over Greenland which are a result of the strong filtering described in Chapter 2 to eliminate spurious variances in regions which contain non-real data. Summer difference maps are not presented as the anomalies noted by Dickson et al. (1975, 1988) were strongest in winter.

Difference maps for sea ice cover show that there was much more ice in the

Barents, Greenland-Iceland and Labrador Seas during the late 1960s than during the decade from 1956-65 (Figure 4.1c). There were also higher ice concentrations in the Greenland-Iceland and Barents Seas in the 1960s than in the 1970s, but less ice in the Davis Strait and the Labrador Sea in the 1960s than in the early 1970s (Figures 4.2d, 4.3d).

4.2 Anomaly maps

Anomaly maps for four year periods beginning in 1963 are presented in this section. Four year averages were used in order to obtain a picture of the atmospheric circulation over timescales long enough to influence large scale (i.e., over the entire Arctic) ice motion, while short enough to still resolve the changes that occurred around the time of the GSA. The averages start in 1963 as this is the first year data are available for 850 hPa temperatures. These maps also separate the circulation in the 1960s, when the high pressure anomaly cell was present over Greenland, and the early 1970s, when the anomalously anticyclonic circulation collapsed and was replaced by an intensified Icelandic Low.

The maximum value of the average winter SLP anomaly with respect to climatology during the period from 1963-1966 was +7 hPa, centred over Iceland (Figure 4.4a). From 1967 to 1970 average maximum winter anomalies were up to +5 hPa over the Irminger Sea and +6 hPa over northern Russia (Figure 4.5a). As noted by Dickson et al. (1975) this anomaly ridge collapsed in 1970 and by the early 1970s was replaced by an intensified Icelandic Low. Average winter SLP anomalies over the Irminger Sea for the period 1971-1974 (Figure 4.6a) were up to -4 hPa. The anomaly maps for winter 500 Z for the same periods are qualitatively very similar, although it is interesting to note that the anomaly map for 1971-1974 is almost the exact negative of the anomaly map for 1967-1970 (see Figures 4.5b and 4.6b). These large scale anomalies suggest Rossby waves, or a largely meridional circulation existed at these times. The summer anomaly fields for SLP and 500 Z (not shown) are all comparatively flat and structureless.

During the 1960s the 850 hPa temperatures were higher than normal over Greenland, Baffin Bay, eastern Canada, and the western Atlantic while they were lower than normal over western Europe and the Arctic Ocean (Figures 4.4c and 4.5c). This is consistent with the idea proposed by Dickson et al. (1975) that increased anticyclonic circulation centred over the Greenland Sea increased the southerly advection of warm air to the west and the northerly advection of cold air to the east. The 500 Z anomaly field (Figure 4.5b) also shows increased cyclonic circulation centred over central Europe from 1967-70, which would further increase the frequency of northerly winds over western Europe. A pool of cold air existed over the central Arctic Ocean from 1967-1970 (Figure 4.5c), which would have enhanced Arctic sea ice formation and contributed to the large amounts of ice exported to the Greenland Sea during this period. This is consistent with Power and Mysak's (1992) discussion (see Chapter 1) concerning the decreased heat transport to the Arctic due to the weakened Icelandic Low, and the resulting increased Arctic sea ice formation.

The sign of the patterns changed in the early 1970s (Figure 4.6c), with below normal temperatures over most of Canada and warmer than normal air over northwestern Europe, again consistent with the now increased cyclonic circulation over the northern North Atlantic advecting warm air to the east and cold air to the west. From the SLP and 500 Z anomaly fields for this period (Figure 4.6a,b), it can be seen that there was increased anticyclonic circulation over Central Europe, which also increased the frequency of warm southerly winds over Western Europe. The colder than normal air to the west, i.e. over Canada in Figure 4.6c, extends far beyond the region one would expect to be influenced by atmospheric circulation patterns over the Atlantic, and there are likely to be other climatic influences which affected Canadian temperatures at this time.

The atmospheric summer anomaly maps are fairly flat, with the exception of the summer 850 T anomaly for 1967-1970, when there is a cold temperature anomaly of up to -1.5°C over the northern Ob Basin (not shown).

The winter sea ice concentration anomaly maps show positive ice concentrations in the Greenland-Iceland Sea throughout the 1960s, peaking in the late 1960s (Figures 4.4d and 4.5d). Positive anomalies are present in the Barents Sea during the late 1960s (Figure 4.5d), and in the Davis Strait and Labrador Sea in the early 1970s (Figure 4.6d). A slight positive anomaly persisted in the Greenland Sea in the early 1970s (Figure 4.6d).

4.3 EOF results

The leading EOF of winter sea ice concentration, representing 23% of the explained variance of sea ice anomalies, describes the main ice concentration anomalies associated with the Great Salinity Anomaly (Figure 4.7 top). The pattern depicts large concentration anomalies in the Greenland and Barents Seas, and ice anomalies of the opposite sign in the Labrador Sea and Davis Strait. This dipole pattern is similar to that found by Fang and Wallace (1994), although they analyzed data only from 1972 to 1989, and used different compositing methods. The pattern is also consistent with the findings of Walsh and Johnson (1979b), who found that their EOF 1 of annual sea ice data described an out of phase relationship between concentrations in the northern North Atlantic, Norwegian and Barents Seas, and the remainder of the polar cap.

The time series of EOF 1 shows large negative values from 1964 to 1971, and then positive values for three years, implying large (small) sea ice extents in the late 1960s (early 1970s) in the Greenland-Iceland Sea. This change in sea ice cover is consistent with the advective hypothesis of ice anomalies associated with the GSA (Mysak et al., 1990), since large sea ice extents and low salinity water mass were present in the Greenland Sea from 1968 to 1971, and subsequently moved to the Labrador Sea and off the coast of Newfoundland in 1971 and 1972. The small negative values of the time series during the late 1970s and early 1980s may represent ice anomalies associated with the return of the GSA to the Greenland Sea.

This EOF also suggests that the ice concentration variability of the Greenland Sea is linked to that of the Barents Sea. It also explains a small amount of variance in ice concentration in the Sea of Okhotsk and the Baltic Sea; the latter signal may be a direct result of the temperature anomalies over Western Europe and Scandinavia. Other EOFs (not shown), while consistent with the large ice anomalies which accompanied the GSA, are not *primarily* associated with the event, as would be expected since by definition the EOFs are mutually orthogonal vectors. The leading pattern of summer sea ice concentration, explaining 33% of the variance in the record (Figure 4.8) does not appear to be dominated by the GSA, but rather by negative ice anomalies in the last two years of the record, a result consistent with the large negative summer sea ice anomalies over the entire Arctic found by Chapman and Walsh (1990). When the last year (1990) is removed from the record, the first EOF of summer sea ice concentration explains only 15% of the variance (Figure 4.9). The time series implies that there are large positive summer sea ice anomalies in the Barents and Kara Seas, as well as in the Greenland Sea, from 1964 to 1970, and large negative anomalies in these regions in the 1970s.

The leading EOF for winter SLP (accounting for 38% of the explained variance) describes a general high or low pressure cell over the polar and subarctic regions with a corresponding centre of opposite sign over Western Europe (Figure 4.10). The pattern is reminiscent of the winter anomaly map for 1967-1970 presented in the previous section (see Figure 4.5a). This EOF pattern is consistent with the results from the EOF analysis presented in Walsh (1978), where the leading EOF of SLP north of 60°N represents a general excess or deficit of mass over the pole. The spatial pattern of EOF 1 of summer SLP (accounting for 27% of the explained variance) is very similar to the spatial structure of EOF 1 of winter SLP (Figure 4.11). The spatial structure of the leading EOF for winter 500 Z (25%) is also similar to the first EOF of winter SLP, but with a more pronounced feature over Western Europe (Figure 4.12). Again, the spatial structure is much like the winter 500 Z anomaly map for the period 1967-1970 (Figure 4.5b). The Western European feature does not appear at all in the pattern of the leading EOF for 500 Z summer (18%), which is otherwise similar in spatial structure to the other patterns described so far (Figure 4.13).

The first EOF for winter 850 T (26%) has a dipole structure over the polar cap with temperature anomalies of one sign over the Pacific, North America, and the western half of the North Atlantic, while anomalies of the opposite sign occur over Eurasia, the eastern North Atlantic and the Arctic (Figure 4.14). This is an extension over the entire hemisphere of the pattern that was observed in the anomaly maps of the 1960s and early 1970s (Figures 4.4c., 4.5c and 4.6c). EOF 1 of summer 850 T does not have a very pronounced pattern: its main feature is a weak see-saw between the sign of anomalies over the polar ocean and those over the surrounding continents (Figure 4.15).

Perhaps not surprisingly, the time series of EOF 1 of winter SLP (Figure 4.10) and winter 500 Z (Figure 4.12) are quite similar (although opposite in sign), as are the time series for the two summer fields (Figures 4.11 and 4.13). The time series for the summer and winter fields are not at all similar, which is surprising as the spatial patterns of both seasons are alike. The winter time series are fairly flat until the 1960s, after which the SLP series tends to oscillate with a period of about 10 years. The winter 500 Z time series is less regular, but has two periods of mainly positive values and two periods of negative values over the span from 1965-1995. The summer 500 Z time series (Figure

4.13), on the other hand, shows relatively large positive values in the 1940s and 50s, then negative values from 1960 until 1975, that is, an interdecadal change. Fairly pronounced decadal oscillations occurred after 1975. The summer SLP time series (Figure 4.11) has a large positive phase in the late 1950s, a strong negative phase in the early 60s, a period of small fluctuations from 1965 until 1976, and finally a phase of 10 year oscillations until 1995.

The time series of the leading winter and summer modes of the temperature fields have little interannual variability as compared to the SLP and 500 Z time series. Instead, the time series of EOF 1 for winter 850 T (Figure 4.14) shows a strong decadal scale oscillation, with three cycles over a period of 32 years. This is consistent with the results of Deser and Blackmon (1993) and Mysak et al. (1996), who found decadal oscillations in more limited areas. The smoothed time series (a three year running mean) of the first EOF of summer 850 T (Figure 4.15) changes sign only once, when the series changes from negative to positive values in 1979.

The fact that the leading EOFs of the atmospheric variables correspond closely to the spatial structure of the atmospheric anomalies during the late 1960s suggests that a large percentage of the explained variance in the atmospheric circulation can be accounted for by changes that occurred around this period. The leading EOF time series of the variables show that the patterns prevalent in the 1960s and early 1970s are generally well defined (implying large anomalies) and long-lived. The relationship between sea ice concentration anomalies and atmospheric circulation changes is explored statistically in the next chapter using cross-correlation techniques.

5. RESULTS OF CORRELATION ANALYSIS

Maps of the temporal correlation between the negative of the time series for EOF 1 of winter sea ice and the winter and summer time series of each atmospheric anomaly field at every grid point were calculated for various lags. The maps are presented and the implications of the results are discussed in this chapter.

5.1 Description of correlation maps

The maps that are presented in this section have all passed Livezey and Chen's (1983) binomial test for field significance at the 95% level (Chapter 3).

As expected from the results discussed in the previous chapter, the sea ice concentration anomalies tend to be more significantly correlated with winter SLP anomalies than with summer SLP anomalies (see Figures 5.1 and 5.3). At a lag of -1 (i.e., the atmosphere leads the ice by one year), there is a large area of significant correlation extending over the Greenland Sea, the Norwegian Sea, the Barents and Kara Seas, and northern Russia (Figure 5.1a). In this as in all other correlation maps, a positive correlation implies the atmospheric anomalies are positive when sea ice anomalies in the Greenland and Barents Seas are positive (i.e. when the time series of EOF 1 of winter sea ice is negative, as in the 1960s). At zero lag, winter SLP over the Greenland Sea, Greenland, and the Canadian Arctic Archipelago (CAA) is significantly correlated with ice anomalies in the Greenland and Barents Seas (Figure 5.1b). Winter SLP over the same general area is still significantly correlated at a lag of +1 (Figure 5.1c), with areas of correlation at 99% significance over both the Irminger Sea and the CAA. The positive lag implies the ice concentration field is leading the SLP anomalies.

The winter 500 Z correlation maps tend to show more of a dipole structure at lags of -1 and zero (Figures 5.2a and 5.2b, respectively), with a centre of negative correlation over southern Greenland and Iceland and a centre of positive correlation over central

Europe. The correlations are much stronger and more widespread at zero lag than at -1 (atmosphere leading ice). At a lag time of +1 (Figure 5.2c), the winter 500 Z correlation map starts to resemble the SLP map at a lag of +1, although the areas of significant correlation are still situated farther south than are those for SLP.

The only summer pressure field that has significant areas of correlation with EOF 1 of winter ice concentration is summer SLP at a lag of +1.5 (Figure 5.3), for which there are areas of significant positive correlation over western and central Russia.

The maps of the correlation between sea ice concentration and 850 temperature have patterns similar to those of the anomaly maps presented in the previous chapter. At a lag of -1, the winter 850 T over the northwestern North Atlantic is significantly positively correlated to the first EOF of ice concentration, while a negative correlation exists between the fields over Scandinavia (Figure 5.4a). At zero lag, the area of significant negative correlation over Scandinavia has spread to include most of northwestern Europe, the Norwegian Sea and the central polar ocean (Figure 5.4b). The area of significant positive correlation is over the same general area as at lag -1, although it has expanded to include the eastern part of the Northwest Territories. At a lag time of one year (Figure 5.4c), the area of positive correlation has diminished to a region over the western Atlantic, while the areas of negative correlation are centred north of the British Isles and over the north pole (Figure 5.4c). The correlation map of ice with summer temperature at a lag of +1/2 (Figure 5.5a) shows areas of significant negative correlation between EOF 1 of sea ice concentration and summer 850 temperatures over central and eastern Canada, western Europe, and northern Russia. Finally, at a lag time of +1.5 years (Figure 5.5b), there are two distinct areas of significant negative correlation, one over Québec and Hudson Bay, the other over northwestern Russia (Figure 5.5b). It is interesting to note that the areas of significant correlation tend to be seasonally coherent. That is to say, the patterns of correlation between EOF 1 of winter sea ice and winter 850 T have similar structures at different time lags, as do the correlation patterns with summer 850 temperatures, but the winter and summer patterns are different.

5.2 Discussion

There are four possible interpretations for a given correlation. A positive correlation implies that when the time series of EOF 1 of winter ice concentration is negative, the sign of the corresponding atmospheric anomaly tends to be positive (as the correlations are calculated between the time series of the atmospheric anomaly fields at each grid point and the *negative* of the time series of EOF 1 of winter sea ice concentration). Thus a positive correlation implies that when ice concentrations in the Greenland and Barents Seas are large, the atmospheric anomalies are high, and when there are low ice extents in the Greenland and Barents Seas, the atmospheric anomalies are negative. At the same time, a positive correlation would also imply that when the ice concentrations in the Labrador Sea and Baffin Bay are large (the time series of EOF 1 of winter ice concentration is positive), the atmospheric anomalies tend to be negative, and when the ice concentrations in these areas are low, the atmospheric anomalies are positive. Opposite arguments hold for negative correlations.

Given that the pattern of EOF 1 of winter ice concentration has such a strong spatial structure in the Greenland and Barents Seas and relatively weak one in the Labrador Sea and Baffin Bay, it is probably best to assume the maps described in the previous section correlate mainly with concentration anomalies in the Greenland and Barents Seas. However, the fact that the sign of the anomaly associated with a positive or negative correlation changes when considering ice anomalies in the Labrador Sea should be kept in mind when interpreting the results of the correlation maps.

There are several ways in which the atmosphere and sea ice can interact with each other and produce the areas of correlation described above. As discussed in Chapter 1, the atmosphere can affect the distribution of sea ice as the surface winds blow over the sea ice, causing the ice to drift in the general direction of the geostrophic wind. Low atmospheric temperatures can also cause the underlying ocean surface to cool and enhance sea ice formation (Walsh, 1978). The presence of sea ice in turn can influence the atmosphere by changing the surface roughness of the underlying surface and affecting momentum transfers, which in turn can have an effect on the strength and direction of the winds (Agnew, 1993). Sea ice also affects the heat transfer from the ocean surface to the atmosphere, a process which is particularly important in winter when the ocean surface is much warmer than the overlying atmosphere.

It is also possible that the correlations are not causal, that is that both the sea ice and the atmospheric circulation are responding to some third factor (such as insolation, for example), and are merely both acting in phase with some other forcing. However, this possibility seems fairly remote given the strength and structure of the correlation patterns.

5.2.1 Correlations between sea ice and atmospheric pressures and heights

The correlation map for SLP at a lag of -1 year (Figure 5.1a) suggests that the positive ice concentration anomalies in the Greenland and Barents Seas are related to prior positive SLP anomalies east of Greenland, over the eastern Atlantic, the Barents and Kara Seas and northern Russia. It is not possible to evaluate the effect over Greenland itself as much of the data over that area was filtered (see Chapter 2). This eastern area of correlation may be due to the fact that EOF 1 of winter ice concentration also accounts for large positive ice anomalies in the Barents Sea around the same time as the GSA in the Greenland Sea; previous studies (Chapter 1) focussed mainly on ice and salinity anomalies in the Greenland Sea only. The -1 year lag correlation map for winter 500 Z (data that has not been filtered) (Figure 5.2a), on the other hand, shows the sea ice anomalies correlating with a positive height anomaly centred over the Denmark Strait, which is consistent with the theory of Dickson et al. (1988). From these maps, it can be seen that there are atmospheric anomalies which significantly lead sea ice anomalies.

The correlation maps of winter SLP and 500 Z at lags of zero and +1 (Figures 5.1b,c and 5.2b,c) show areas of significant positive correlation over Greenland, the Western Atlantic and in the case of SLP, the Canadian Arctic Archipelago. The fact that correlation patterns at lag times of zero and +1 (for all atmospheric fields) are significantly different or stronger than the correlation patterns at lag -1 suggests that the presence of the ice anomalies has a significant effect on the atmosphere. The lag +1 map for winter SLP shows that positive ice anomalies in the Greenland-Iceland Sea are significantly correlated with subsequent high pressure anomalies (i.e. decreased cyclones or increased anticyclone frequency) in the Canadian Arctic as well as over the Irminger Sea, and negative ice anomalies are correlated with subsequent low SLP, as hypothesized by Mysak et al. (1990) and Mysak and Power (1992).

Although the late 1950s and 1960s are recognized as being periods of above average pressure in the Greenland region, some of the strongest positive pressure anomalies occurred in the late 1960s, at a time when positive ice anomalies were already established in the Greenland Sea (Mysak and Manak 1989; Figures 4.4 and 4.5). It is possible that a positive feedback effect occurred between the sea ice cover and the atmospheric pressure. The high pressure anomaly may have advected larger than usual amounts of the thick, multi-year sea ice found north of Greenland and Ellesmere Island into the Greenland and Barents Seas (Walsh and Chapman, 1990). This export of thicker ice (see Chapter 1) could have led to ice concentration anomalies over a period of several years, since much of the ice exported to the Greenland and Barents Seas in winter would have melted during the summer, producing a layer of fresh, cool low density water. This layer would persist, as vertical mixing would be suppressed by the low density of the water, and would freeze the following winter, producing large ice extents in the Greenland and Barents Seas. The large ice extents would reduce the heat transfer from the warm winter ocean to the overlying air, creating a cold temperature anomaly (Figure 4.5c). This temperature anomaly in turn may have created an anomalous high pressure cell, analogous to those that occur over the continental land masses in winter (the Canadian and Siberian Highs), further increasing the original high pressure anomaly and completing the loop. This anomalous high pressure cell eventually exported the excess ice into the Atlantic Ocean where the ice and salinity anomalies were caught up in the sub-polar gyre and advected around the northern North Atlantic as the GSA. Once the ice anomalies left the Greenland and Barents Seas, the increased heat transfer from the ocean could have eradicated the cold anomaly allowing the circulation over the northern North Atlantic to return to its usual level of cyclonic circulation (Figure 4.6). The questions that remain are what caused the original high pressure anomaly in the late 1950s, and what caused the change in ice concentration anomalies and atmospheric circulation anomalies in the northern North Atlantic area in the early 1970s? With regard to the latter question, two possibilities are considered here. One is that most of the thick, multi-year ice had already been transported out from the area north of Greenland by the late 1960s, and what remained to be exported was thinner, first year ice. The other possibility is that the ice anomaly itself modified the atmospheric circulation so as to reduce the export of Arctic ice to the Greenland Sea, and instead enhanced the export of ice from the Greenland Sea to the subarctic gyre (see Figure 4.6d). A further evaluation of these possible mechanisms is needed to fully explore the dynamics and thermodynamics of these interactions, and is beyond the scope of this work.

There is no immediate explanation for the processes which might account for the link between the presence of sea ice in the Greenland and Barents Seas and high pressures 18 months later over northern Russia (Figure 5.3). It is possible that this reflects a downstream effect, if the atmospheric anomalies associated with the GSA were advected eastward. S. Lappo (personal communication, 1995) has discovered significant changes in the climate of Russia in the years following large positive ice concentration anomalies in the northern North Atlantic.

5.2.2 Correlations between sea ice and atmospheric temperature

The winter temperature and sea ice correlation maps can perhaps be best explained as a "one step removed" correlation between temperature and pressure anomalies. The winter temperature anomalies are for the most part a result of the atmospheric circulation anomalies, and may only relate to sea ice anomalies because the sea ice itself is correlated with atmospheric circulation anomalies. There are no significant correlations at lag -1 year (i.e. atmosphere leading ice) between temperature and sea ice cover in those areas where the sea ice anomalies occur, that is, over the Greenland-Iceland and Barents Seas. This implies that ice anomalies in the Greenland and Barents Seas are indeed primarily the results of advection of ice into these areas, and not enhanced *in situ* formation due to low air temperatures over these regions. Only at a lag time of zero, i.e. only when ice is already present, does the temperature decrease over some of the regions where the ice anomalies occur, such as over the Fram Strait (Figure 5.4b). However, because the atmospheric fields are not themselves independent (for example, temperature can depend on the state of the circulation, as seen in Chapter 4), it is not possible to separate the thermal effects from the dynamical effects when evaluating the influence of the atmospheric circulation on sea ice cover, or vice versa (Walsh and Johnson, 1979b).

The patterns of the temperature correlations match the regions of cold and warm winter conditions brought about by enhanced temperature advection due to anomalously anticyclonic circulation over the northern North Atlantic, as previously described in Chapter 4. The area of correlation between (low) temperatures and ice concentration situated over the north pole at lag times of zero and +1 (Figures 5.4b,c) may be caused by reduced northward heat transport into the wintertime Arctic. It is possible, for example, that the presence of the high pressure anomaly cell over the northern North Atlantic deflected storm tracks further south and decreased the meridional eddy heat transport, as previously discussed in Chapters 1 and 4..

The maps of summer 850 T correlation indicate that winter sea ice anomalies are highly correlated with the subsequent low summer temperatures at a lag of six and 18 months (Figures 5.5a,b). As there are no maps of corresponding significant correlation in the summer SLP or 500 Z fields, the summer temperature correlations cannot be explained as a result of anomalous temperature advection by the atmospheric circulation anomalies. It is possible that the ice which melts in summer produces a layer of cool fresh water over the northern North Atlantic that is sufficient to cool the overlying air through heat, moisture and momentum exchanges, and this cool air subsequently spreads both eastward and westward over North America and Western Europe, or southward from the Barents Sea in the case of northern Russia.

5.2.3 Correlations at longer leads and lags (Speculative results)

Remarkably, some correlations were found at atmospheric leads of five years and atmospheric lags of four and five years. (No significant areas of correlation were found at lags or leads of 2, 2.5, 3 or 3.5 years.) Large positive ice anomalies in the Greenland and Barents Seas and significantly correlated with below average sea level pressures over the Ob basin in northwestern Russia, and low heights over the Barents Sea and part of the Arctic Ocean five years earlier (Figures 5.6a,b). These maps could also be interpreted as indicating that five years before there were large negative anomalies in the Greenland

and Barents Seas (i.e. in the early 1970s) there were large positive pressure and height anomalies, which is consistent with what has been previously discussed in Chapters 1 and 4. If the low SLP anomalies indicate increased storminess and enhanced precipitation, the latter might cause increased runoff into the eastern Arctic Ocean and hence ice anomalies that appear in the Greenland Sea about 5 years later. This is similar to what Mysak and Power, (1992) showed for western Arctic runoff and the subsequent appearance of sea ice anomalies in the Greenland Sea.

Some significant correlations were also found at long positive lags (atmosphere lags ice) which for the most part describe correlations between the ice concentration anomalies in the northern North Atlantic and atmospheric conditions over the northern Pacific and western North America (Figures 5.7a,b). As it has been fairly well established (van Loon and Rogers 1978; Rogers 1984) that there exist anticorrelated variations in the strengths of the Aleutian and Icelandic Lows, these correlations may simply reflect some teleconnection or see-saw between the two low pressure centres. There are also some areas over Scandinavia and western Russia for summer SLP which are significantly correlated with ice concentration at a lag of +4.

6. CONCLUSIONS

A summary of the main conclusions is presented in this chapter. The thesis as a whole should be taken as a preliminary investigation into the nature of the interactions between the Arctic sea ice cover and the atmospheric circulation at interannual and longer timescales. It is not the intent of this research to provide complete dynamical explanations of the mechanisms of these interactions, but rather to explore the possibility of the existence of such interactions.

Perhaps the first result of interest presented in this thesis is the extension of the sea level pressure (SLP) difference maps, similar to those presented by Dickson et al. (1975) in Chapter 4. The high pressure anomaly cell in winter SLP over Greenland and the Greenland Sea in the 1960s was present, but positive pressure and 500 hPa geopotential height anomalies were also prevalent over most of the Arctic region, particularly over northern Russia, at this time. At the same time, pressures and heights were low over western Europe. The high pressure anomaly cell over Greenland and the northern North Atlantic was replaced in the early 1970s by intensely cyclonic winter circulation, as described by Dickson et al. (1975). In the analysis presented in this thesis, this phenomenon extended also to the 500 hPa height field in the early 1970s, when low heights were observed over Canada, the northwestern North Atlantic, and central Russia, while positive height anomalies existed over central Europe. Thus the circulation anomalies noted over the northern North Atlantic were widespread and in fact extended over much of the Arctic and subarctic region.

The second result of interest is the fact that the first EOF of winter sea ice concentration primarily reflects the ice anomalies associated with the Great Salinity Anomaly (GSA) of 1968-82. This suggests that a large portion of the interannual and longer timescale variability in the sea ice record can be accounted for by the positive anomalies associated with the GSA. The time series of the first EOFs of the wintertime atmospheric variables presented in Chapter 4 also show that the atmospheric circulation anomalies that existed around the time of the GSA account for some considerable portion of the variability in the pressure, height and temperature records since 1947 (1963 for temperature). Altogether, the EOF analyses suggest that the ice and atmospheric circulation anomalies associated with the GSA account for a substantial portion of the variability in the mid to high latitude climate signal. These anomalies in the sea ice concentration and atmospheric variables, as described by the leading EOFs, are among the strongest observed in the post World War II era.

Finally, the correlation maps presented in Chapter 5 raise some intriguing questions as to the precise nature of atmosphere-sea ice interactions. It has been fairly well established (Fang and Wallace, 1994) that at shorter timescales (i.e., weeks) the atmosphere drives the sea ice through the effects of pressure gradients and surface winds directing the motion of sea ice drift. From the results of the correlation maps presented here the conclusion is drawn that at longer (i.e. interannual) timescales there are as many, if not more, statistically significant correlations between ice concentrations in the Greenland and Barents Seas and atmospheric variables when the ice leads the atmosphere as there are vice versa. One possible interaction between sea ice and atmospheric pressure involves a positive feedback described in detail in Chapter 5, where high pressure anomalies in the northern North Atlantic increase the amount of sea ice exported from the Arctic into that region. The ice in turn creates cold air temperature anomalies and enhances the high pressure anomaly in a manner similar to that which creates the winter continental highs over Canada and Siberia. The geostrophic winds associated with the high pressure anomaly eventually export the ice to lower latitudes. The now reduced ice cover enhances the heat transfer from the ocean to the atmosphere, increasing cyclogenesis and creating a low pressure anomaly in that region.

The fact that there are widespread areas of significant correlation between ice anomalies in the Greenland and Barents Seas and the atmospheric anomalies at ice leads of up to 1.5 years provides some evidence that the presence of sea ice can influence atmospheric circulation and temperatures for up to 18 months. The speculations in Chapter 1 regarding the influence of sea ice anomalies on atmospheric temperature and pressure would appear to be substantiated by the correlation maps. Sea ice anomalies in the Greenland and Barents Seas are significantly correlated with low temperatures over the northern North Atlantic and surrounding regions, and with increased SLP over the Irminger Basin and the Canadian Arctic Archipelago. Further research is needed to identify possible mechanisms for these interannual interactions between sea ice concentration and atmospheric circulation.

Correlations between the atmosphere and winter sea ice also exist at longer leads and lags. At an ice lag of 5 years positive correlations exist between the ice and the pressure and height fields over northern Russia and the Barents sea. At an ice lead of 4 years, some statistically significant correlations exist between sea ice extent in the Greenland and Barents Seas and SLP over Scandinavia and western Russia, while at an ice lead of 5 years, areas of significant correlation are found between sea ice cover and circulation and temperature anomalies over the northern Pacific and western North America. Again, further research is needed to explore the possible mechanisms which might produce these correlations at leads and lags of 4 and 5 years.

The results presented in this thesis suggest that much remains to explored in interannual and longer timescale interactions between sea ice and atmospheric circulation. It is by no means certain that sea ice is driven by atmospheric circulation on longer timescales. Rather, it seems likely that the presence of sea ice and changes in the atmospheric circulation both affect the other, and interact with each other in a manner which may be very important for the study of mid and high latitude interannual to decadal scale variability. The physical processes which explain these interactions need to be researched.

REFERENCES

Agnew, T., 1993. Simultaneous winter sea-ice and atmospheric circulation anomaly patterns. *Atmosphere-Ocean*, 31, 259-280.

Bradley, R.S. and J. England, 1978. Recent climatic fluctuations of the Canadian high Arctic and their significance for glaciology. *Arctic and Alpine Research*, 10, 715-731.

Chapman, W.L. and J.E. Walsh, 1993. Recent variations of sea ice and air temperature in high latitudes. *Bulletin of the American Meteorological Society*, 74, 33-47.

Deser, C. and M.L. Blackmon, 1993. Surface climate variations over the North Atlantic Ocean during winter: 1900-1989. *Journal of Climate*, 6, 1743-1753.

Dickson, R.R., H.H. Lamb, S.A. Malmberg, and J.M. Colebrooke, 1975. Climatic reversal in the northern North Atlantic. *Nature*, 256, 479-482.

Dickson, R.R., J. Meincke, S.A. Malmberg and A.J. Lee, 1988. The "Great Salinity Anomaly" in the northern North Atlantic, 1968-1982. *Progress in Oceanography*, 20, 103-151.

Fang, Z. and J.M. Wallace, 1994. Arctic sea ice variability on a timescale of weeks and its relation to atmospheric forcing. *Journal of Climate*, 7, 1897-1913.

Häkkinen, S., 1993. An Arctic source for the Great Salinity Anomaly: a simulation of the Arctic ice-ocean system for 1955-1975. *Journal of Geophysical Research*, 98, 16397-16410.

Jenne, R., 1970. The NMC octagonal grid, National Center for Atmospheric Research, Boulder, Colorado. 22pp.

Lazier, J.R.N., 1980. Oceanographic conditions at Ocean Weather Ship *Bravo*, 1964-1974. *Atmosphere-Ocean*, 18, 227-238.

Livezey, R.E. and W.Y. Chen, 1983. Statistical field significance and its determination by Monte Carlo Techniques. *Monthly Weather Review*, 111, 46-59.

Marsden, R.F., L.A. Mysak and R.A. Myers, 1991. Evidence for stability enhancement of sea ice in the Greenland and Labrador Seas. *Journal of Geophysical Research*, 96, 4783-4790.

Mendenhall, W., D.D. Wackerly and R.L. Scheaffer, 1990. Mathematical Statistics with Applications, PWS-Kent, Boston, MA, pp. 818.

Mysak, L.A. and D.K. Manak, 1989. Arctic sea-ice extent and anomalies, 1953-1984. *Atmosphere-Ocean*, 27, 376-405.

Mysak, L.A., D.K. Manak and R.F. Marsden, 1990. Sea ice anomalies observed in the Greenland and Labrador Seas during 1901-1984 and their relation to an interdecadal Arctic climate cycle. *Climate Dynamics*, 5, 111-133.

Mysak, L.A. and S.B. Power, 1992. Sea-ice anomalies in the western Arctic and Greenland-Iceland Sea and their relation to an interdecadal climate cycle. *Climatological Bulletin*, 26, 147-176.

Mysak, L.A., R.G. Ingram, J. Wang and A. van der Baaren, 1996. The anomalous sea ice extent in Hudson Bay, Baffin Bay and the Labrador Sea during three simultaneous ENSO and NAO episodes . *Atmosphere-Ocean*, 34, in press.

Peixoto, J.P. and A.H. Oort, 1992. Physics of Climate, American Institute of Physics, New York, NY, pp. 520.

Power, S.B. and L.A. Mysak, 1992. On the interannual variability of Arctic sea-level pressure and sea ice. *Atmosphere-ocean*, 30, 551-577.

Roger, J.C., 1984. The association between the North Atlantic oscillation and the Southern Oscillation in the Northern Hemisphere. *Monthly Weather Review*, 112, 1999-2015.

Serreze, M.C., J.A. Maslanik, R.G. Barry, and T.L. Demaria, 1992. Winter atmospheric circulation in the Arctic Basin and possible relationships to the Great Salinity Anomaly in the northern North Atlantic. *Geophysical Research Letters*, 19, 293-296.

Serreze, M.C., J.E. Box, R.G. Barry and J.E. Walsh, 1993. Characteristics of Arctic synoptic activity, 1952-1989. *Meteorology and Atmospheric Physics*, 51, 147-164.

Serreze, M.C., 1995. Climatological aspects of cyclone development and decay in the Arctic. *Atmosphere-Ocean*, 33, 1-23.

van Loon, H., and J.C. Rogers, 1978. The seesaw in winter temperatures between Greenland and northern Europe. Part I: General description. *Monthly Weather Review*, 106, 296-310.

Walsh, J.E., 1978. Temporal and spatial scales of the Arctic circulation. *Monthly Weather Review*, 106, 1532-1544.

Walsh, J.E. and C.M. Johnson, 1979a. Interannual atmospheric variability and associated fluctuations in Arctic sea ice extent. *Journal of Geophysical Research*, 84, 6915-6928.

Walsh, J.E. and C.M. Johnson, 1979b. An analysis of Arctic sea ice fluctuations, 1953-77. *Journal of Physical Oceanography*, 9, 580-590.

Walsh, J.E. and W.L. Chapman, 1990a. Short-term climatic variability of the Arctic. *Journal of Climate*, 3, 237-250.

Walsh, J.E. and W.L. Chapman, 1990b. Arctic contribution to upper-ocean variability in the North Atlantic. *Journal of Climate*, 3, 1462-1473.

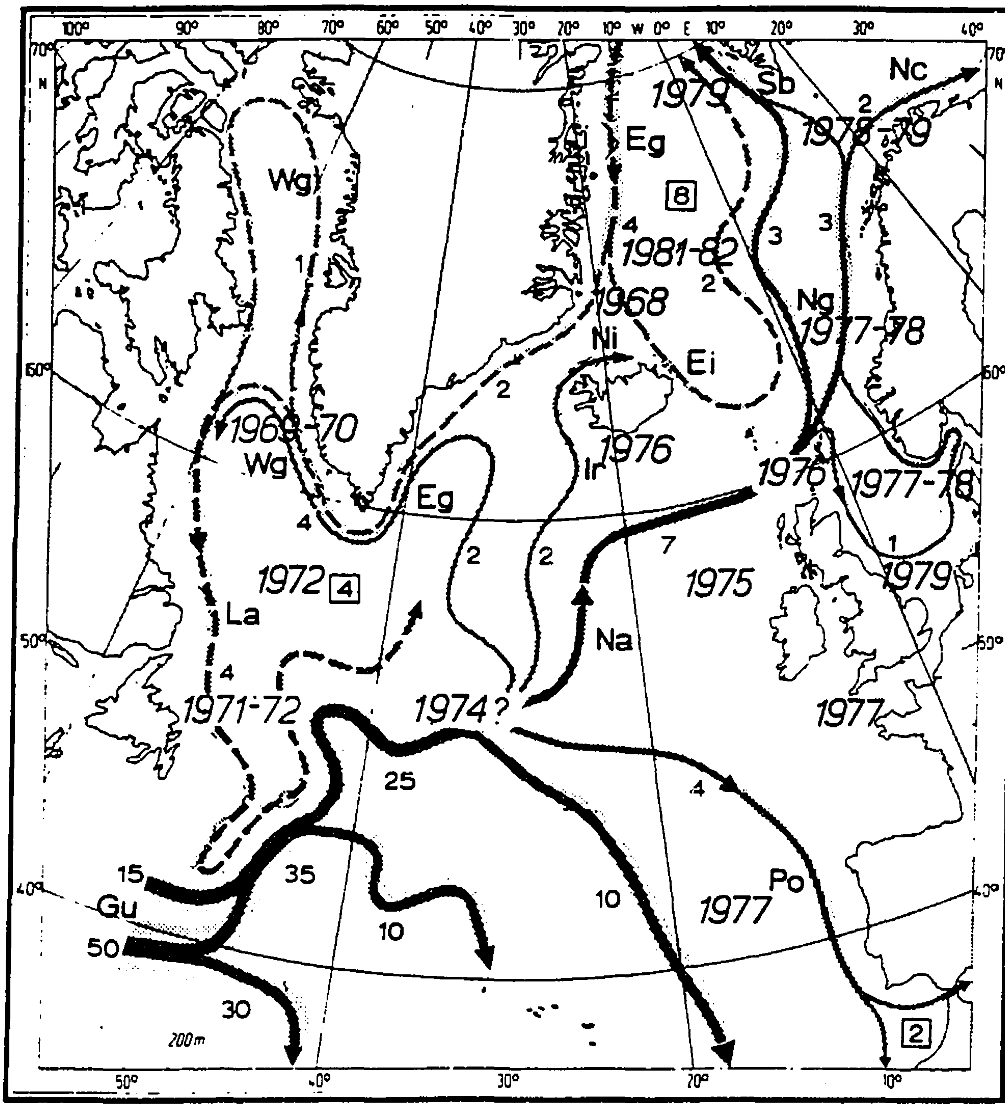

Figure 1.1 Map depicting the transport scheme (currents) of the upper layer of the northern North Atlantic, with the dates of observed salinity minima associated with the Great Salinity Anomaly superimposed. From Dickson et al. (1988).

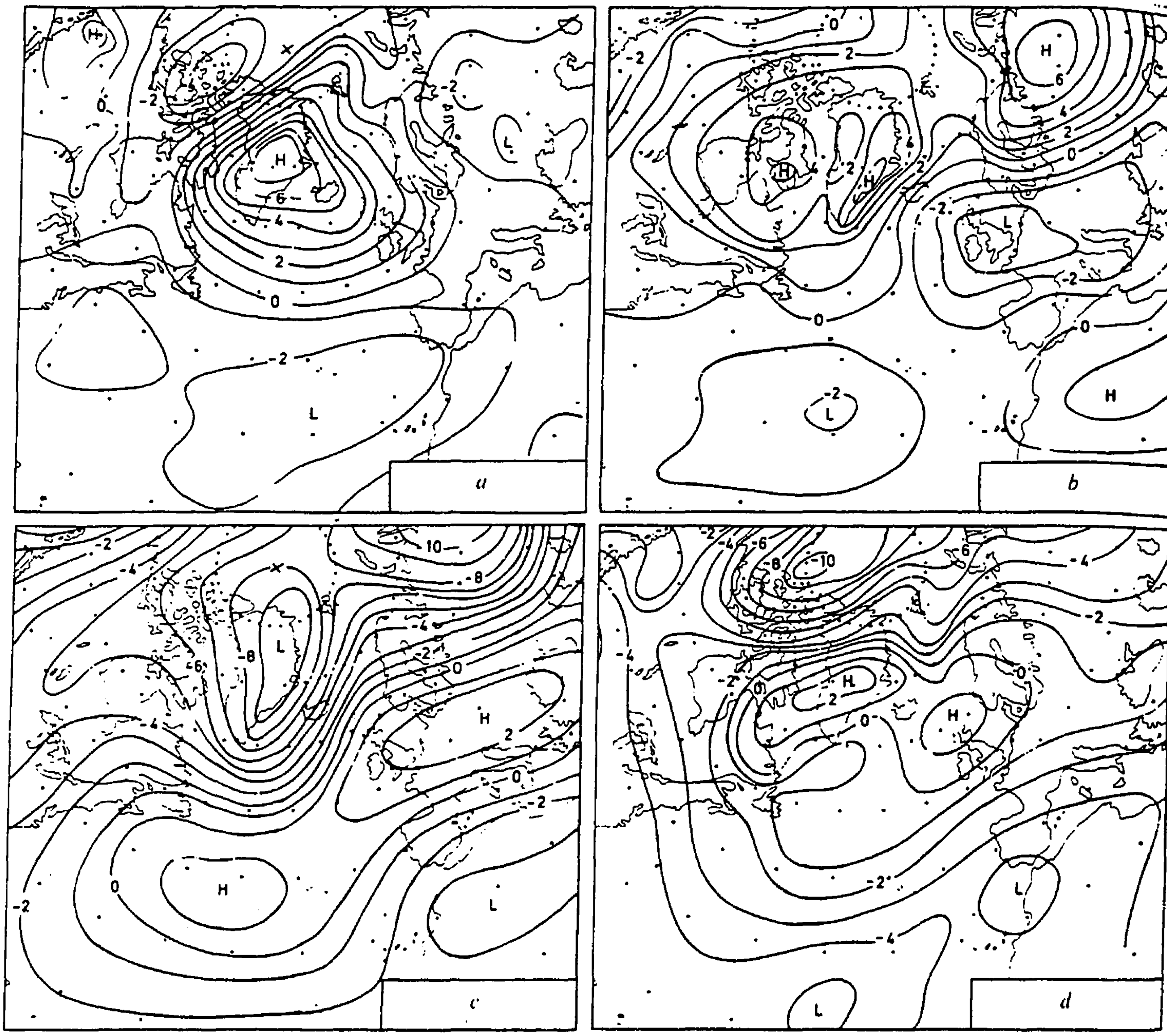

Figure 1.2 Maps depicting the change in mean winter sea level pressure in hPa between a) 1900-39 and 1956-65, b) 1956-65 and 1966-70, c) 1966-70 and 1971-74, and d) 1900-39 and 1971-74. From Dickson et al. (1975).

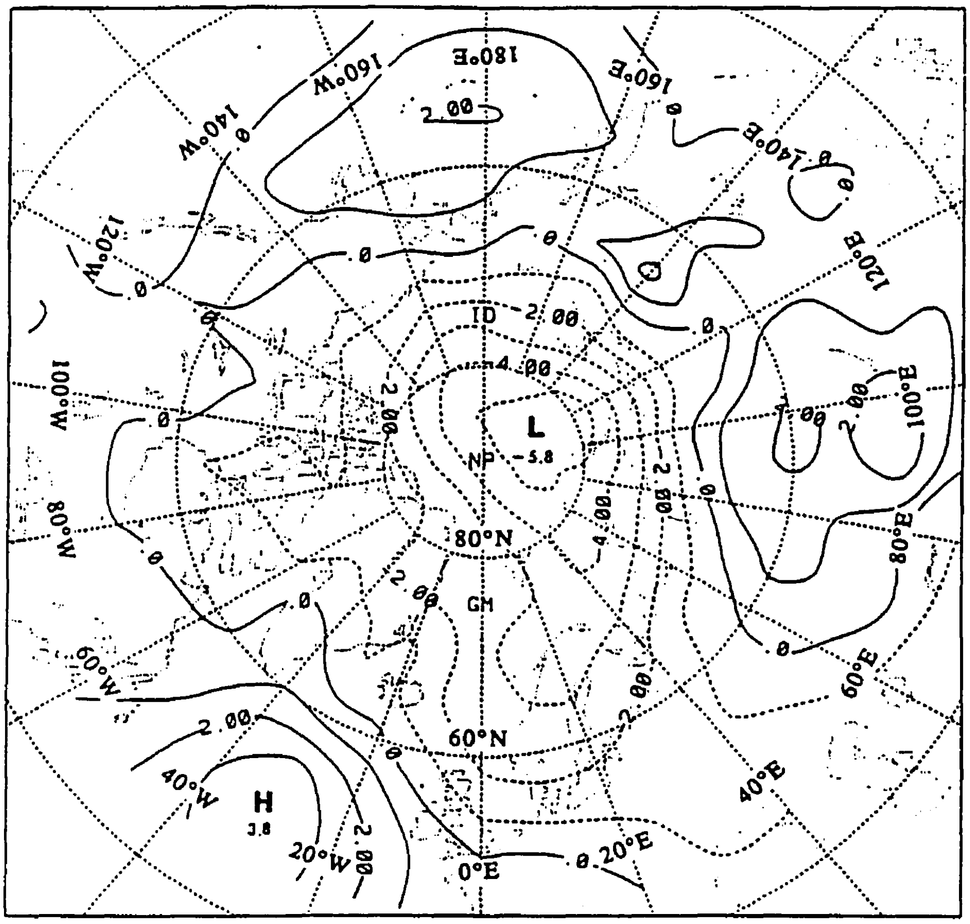

Figure 1.3 April 1967 to March 1968 mean departure (in hPa) from the post-1940 climatology. From Walsh and Chapman (1990).

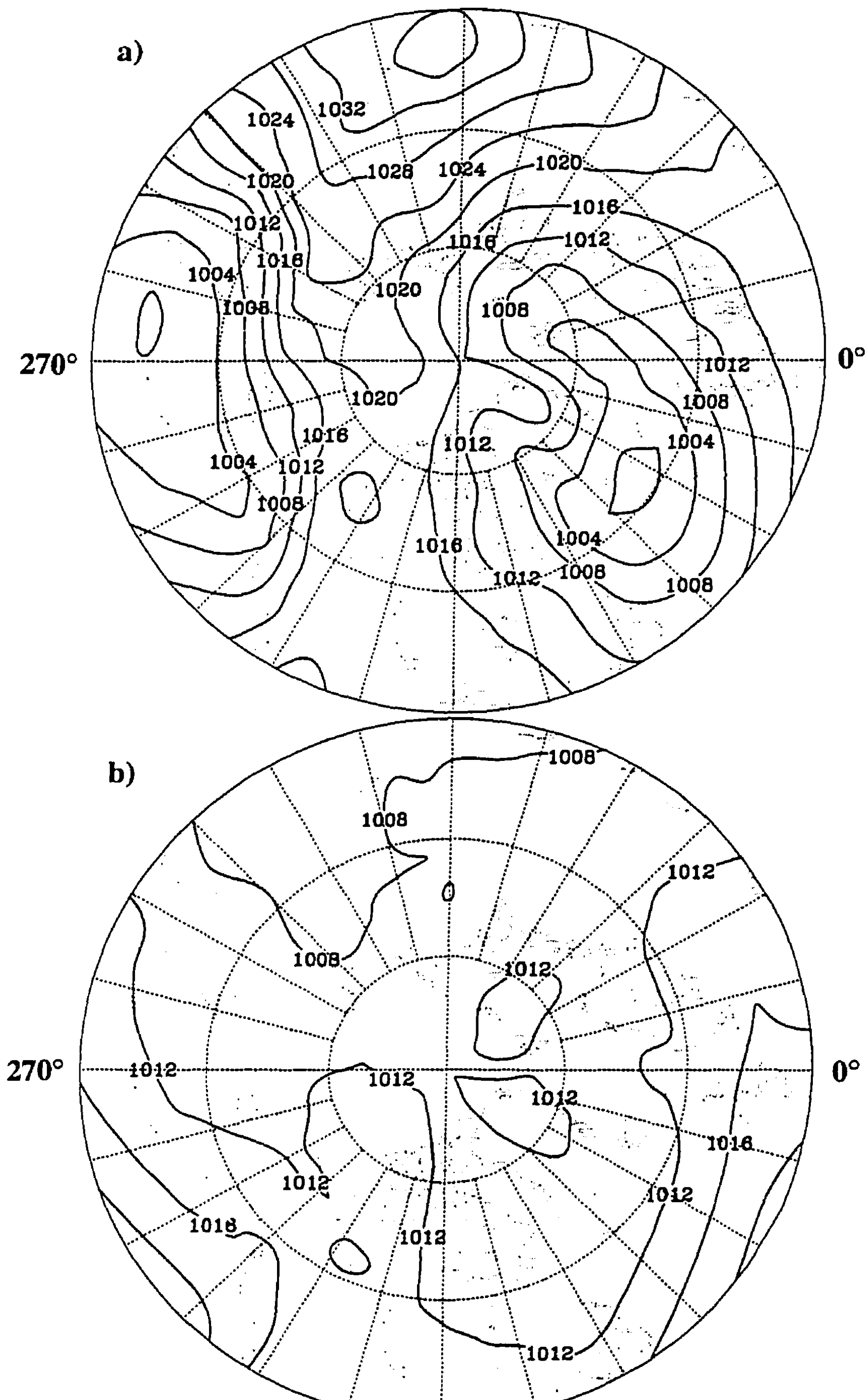

Figure 2.1 Sea level pressure climatology in hPa for 1947-1994 for a) winter and b) summer. Contour interval is 4 hPa.

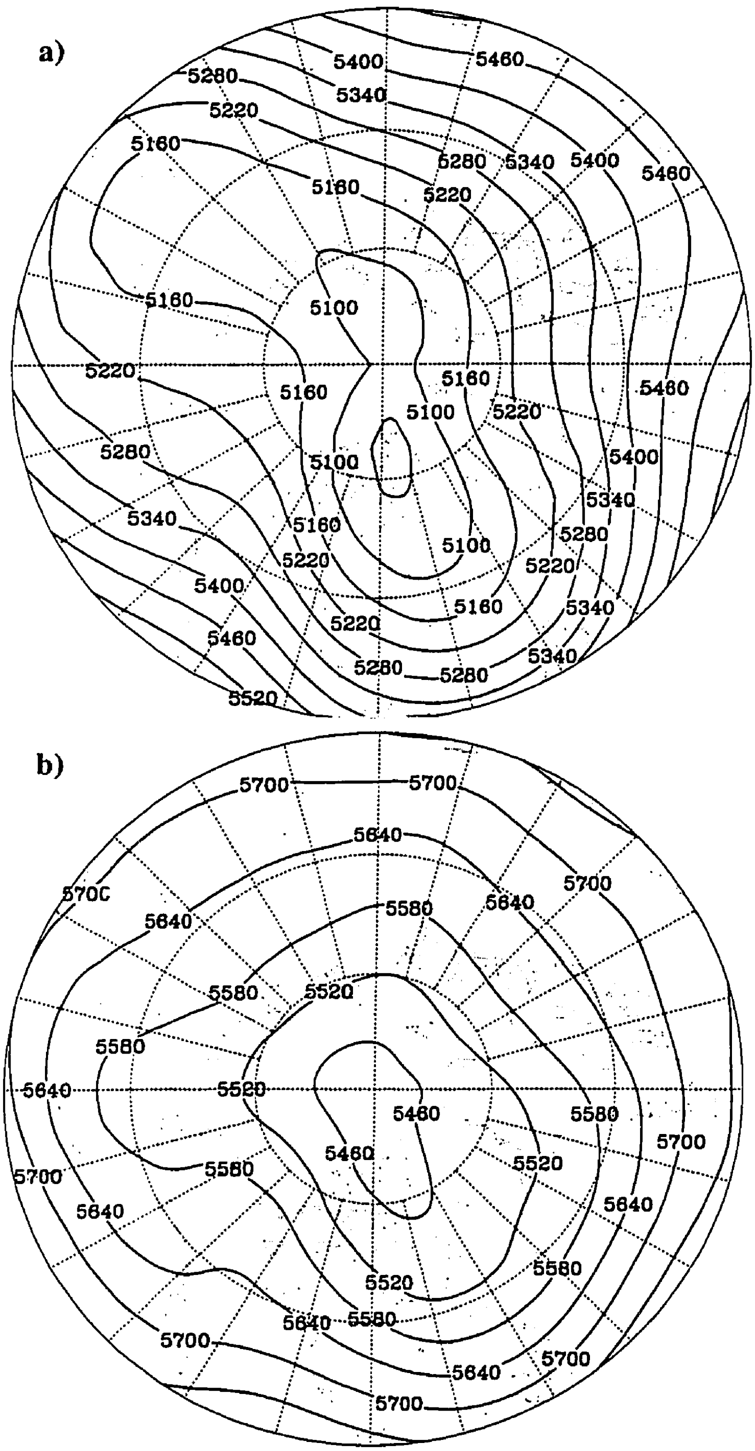

Figure 2.2 500 hPa geopotential height climatology in m for 1947-1994 for a) winter and b) summer. Contour interval is 60 m.

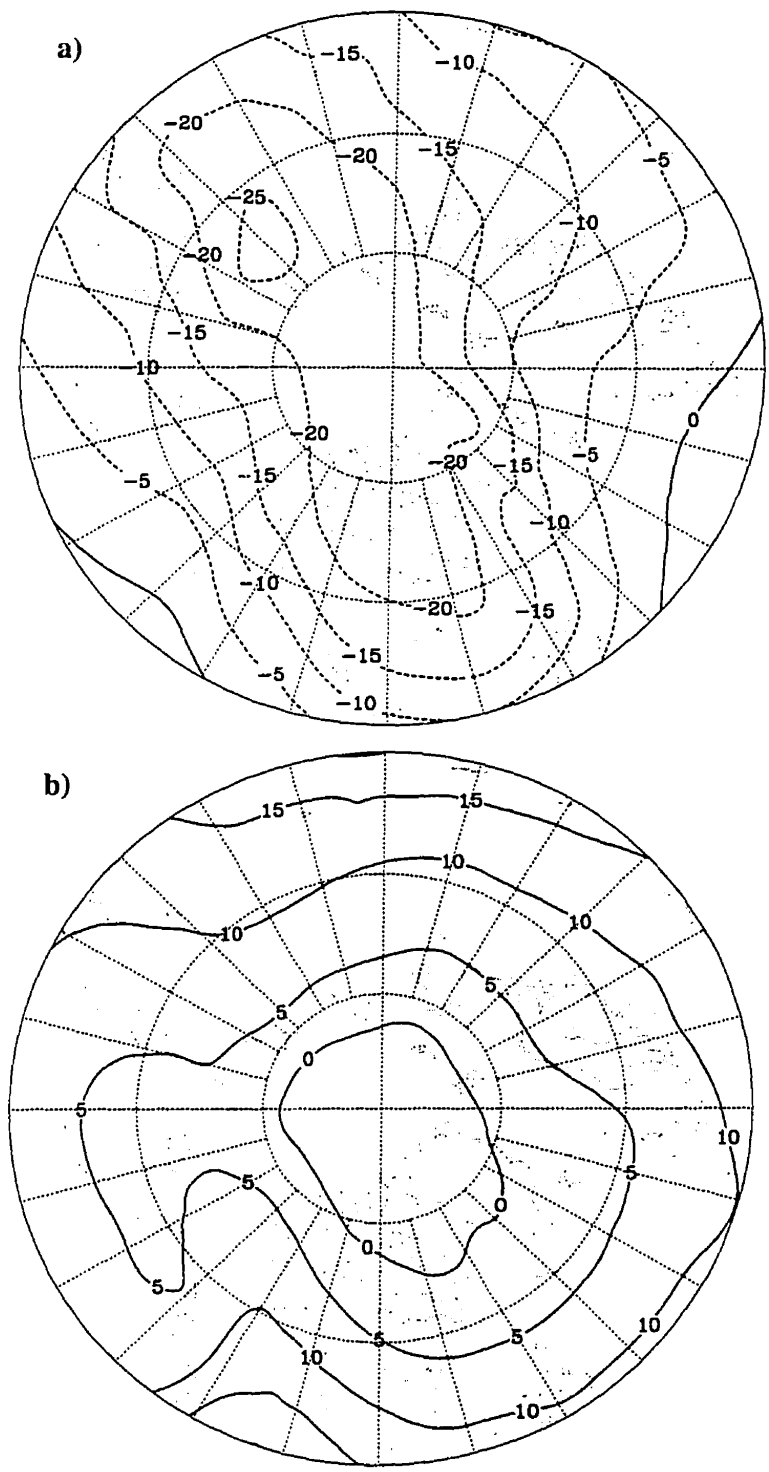

Figure 2.3 850 hPa temperature climatology in °C for 1963-1994 for a) winter and b) summer. Contour interval is 5°C.

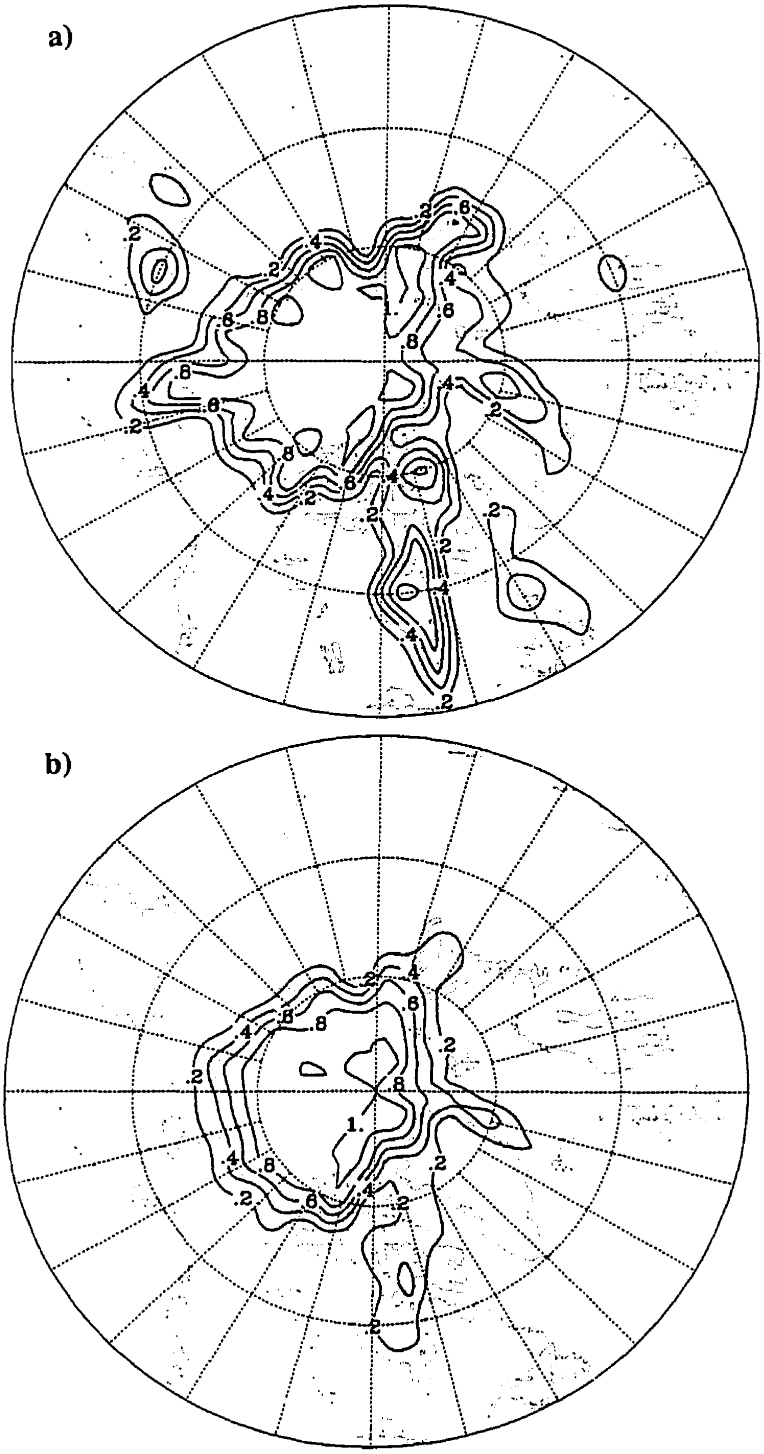

Figure 2.4 Sea ice concentration climatology in tenths for 1954-1990 for a) winter and b) summer. Contour interval is 0.2. Note the contour lines occasionally overlap onto the continents; this is an artifact of the contouring routine.

a)

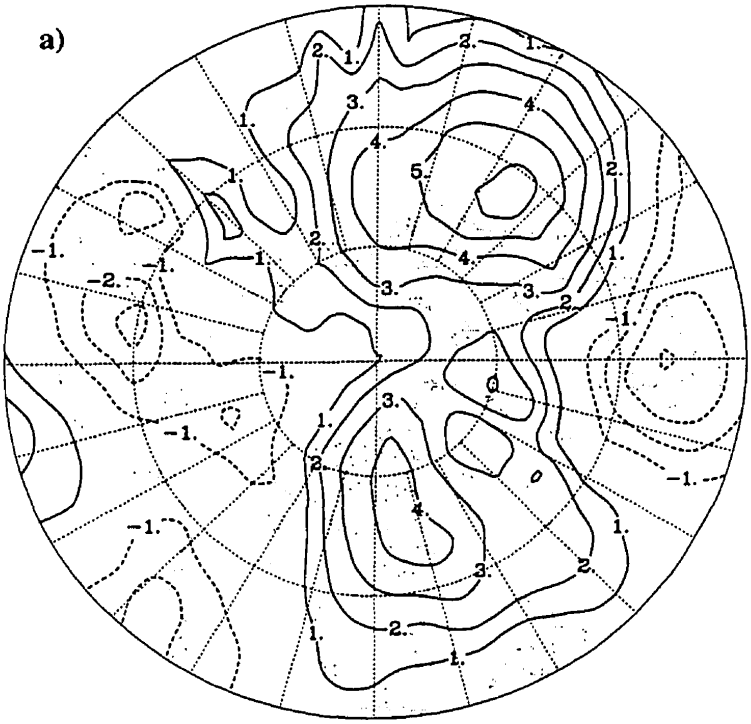

b)

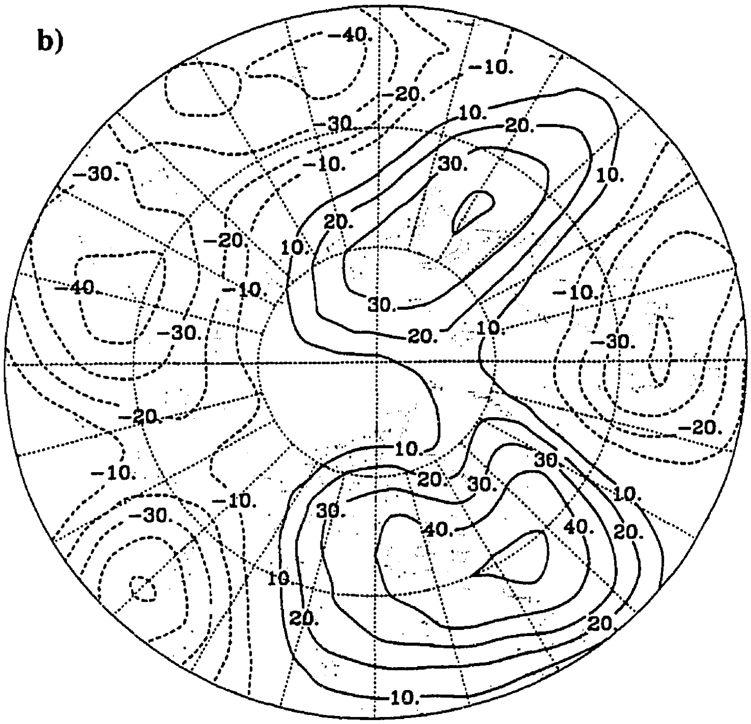

Figure 4.1 Maps of differences between 1956-65 and 1966-70 for a) SLP (in hPa), b) 500 Z (in m) and c) sea ice concentration (in tenths). Note that in this as in the next two figures, the maps represent the earlier (i.e., 1956-65) period subtracted from the later period.

c)

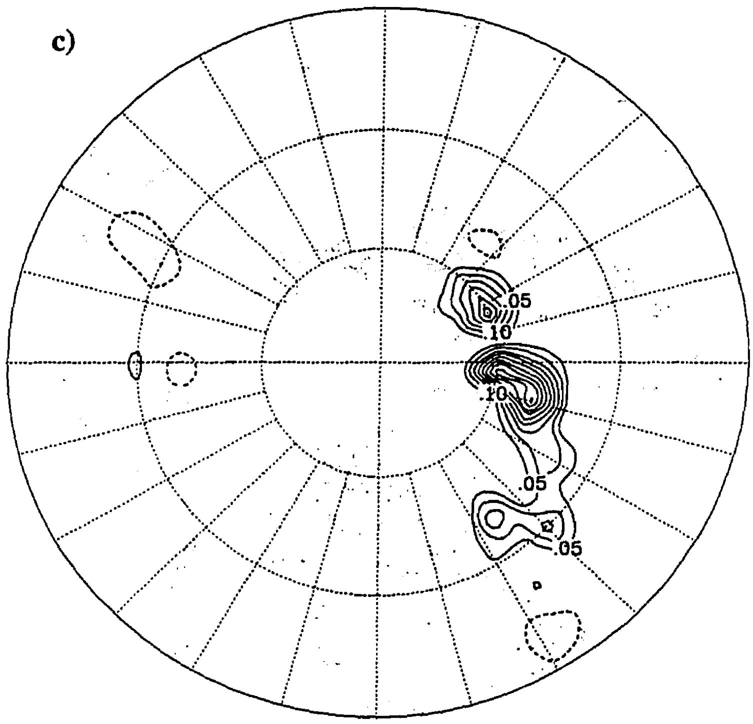

Figure 4.1 cont'd.

a)

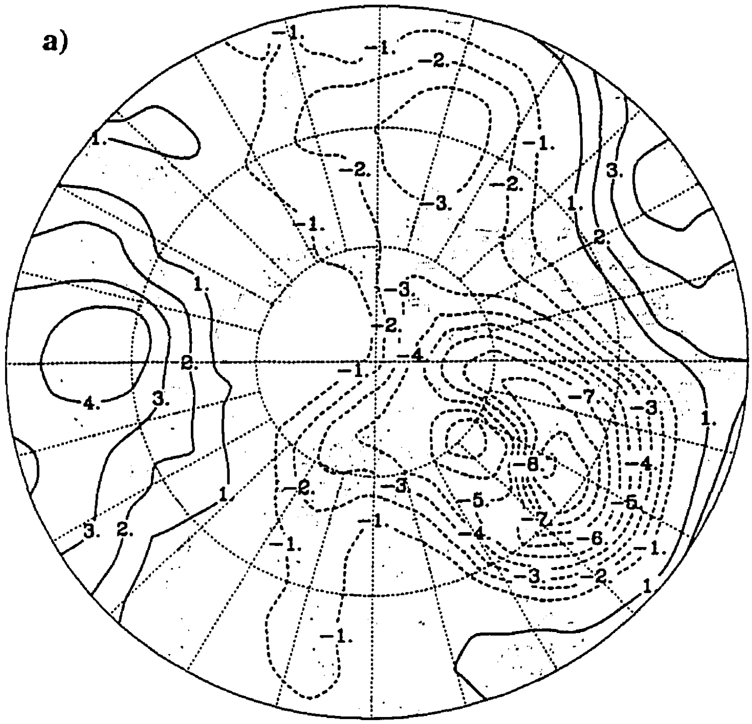

b)

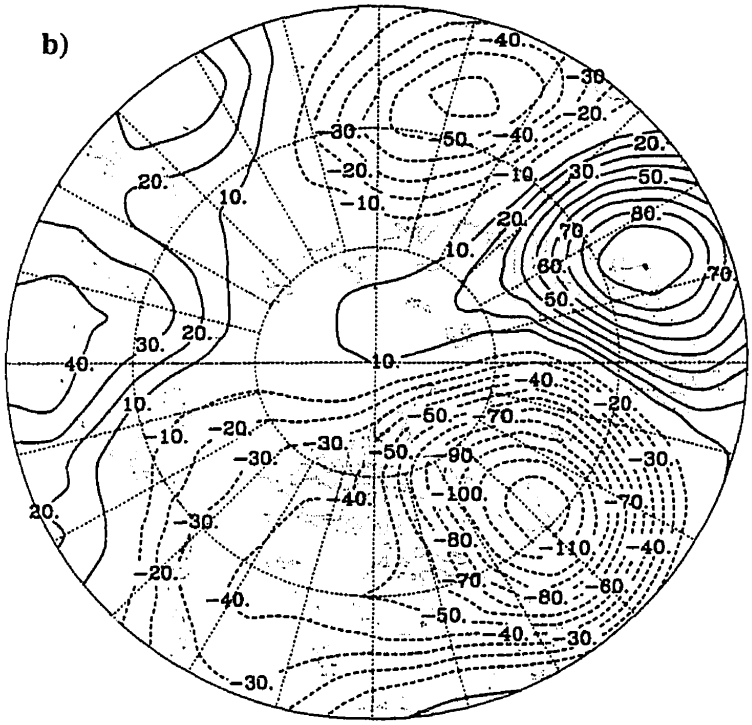

Figure 4.2 Differences between 1963-70 and 1971-74 for a) SLP (in hPa), b) 500 Z (in m), c) 850 T (in °C) and d) sea ice concentration (in tenths).

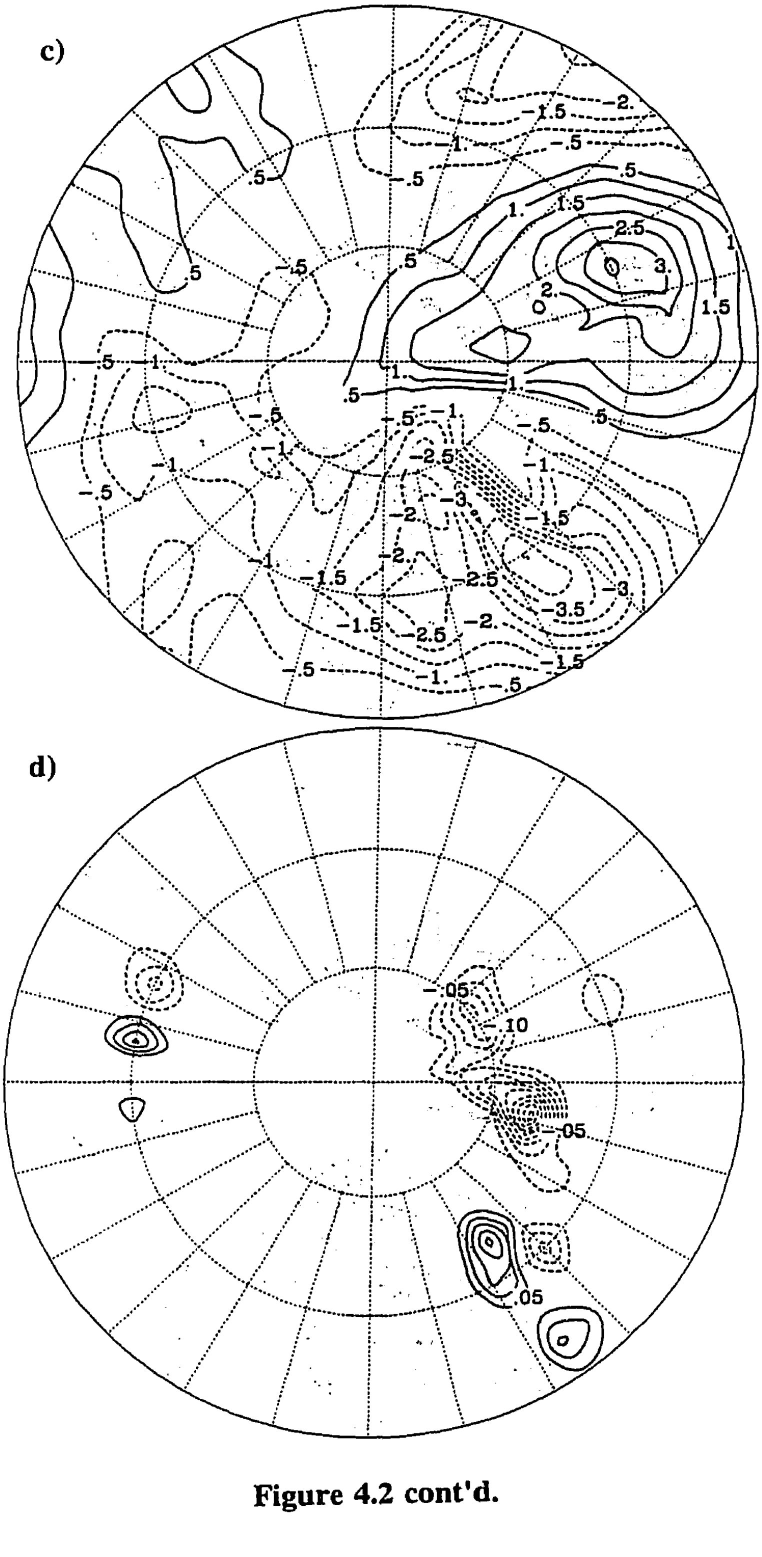

Figure 4.2 cont'd.

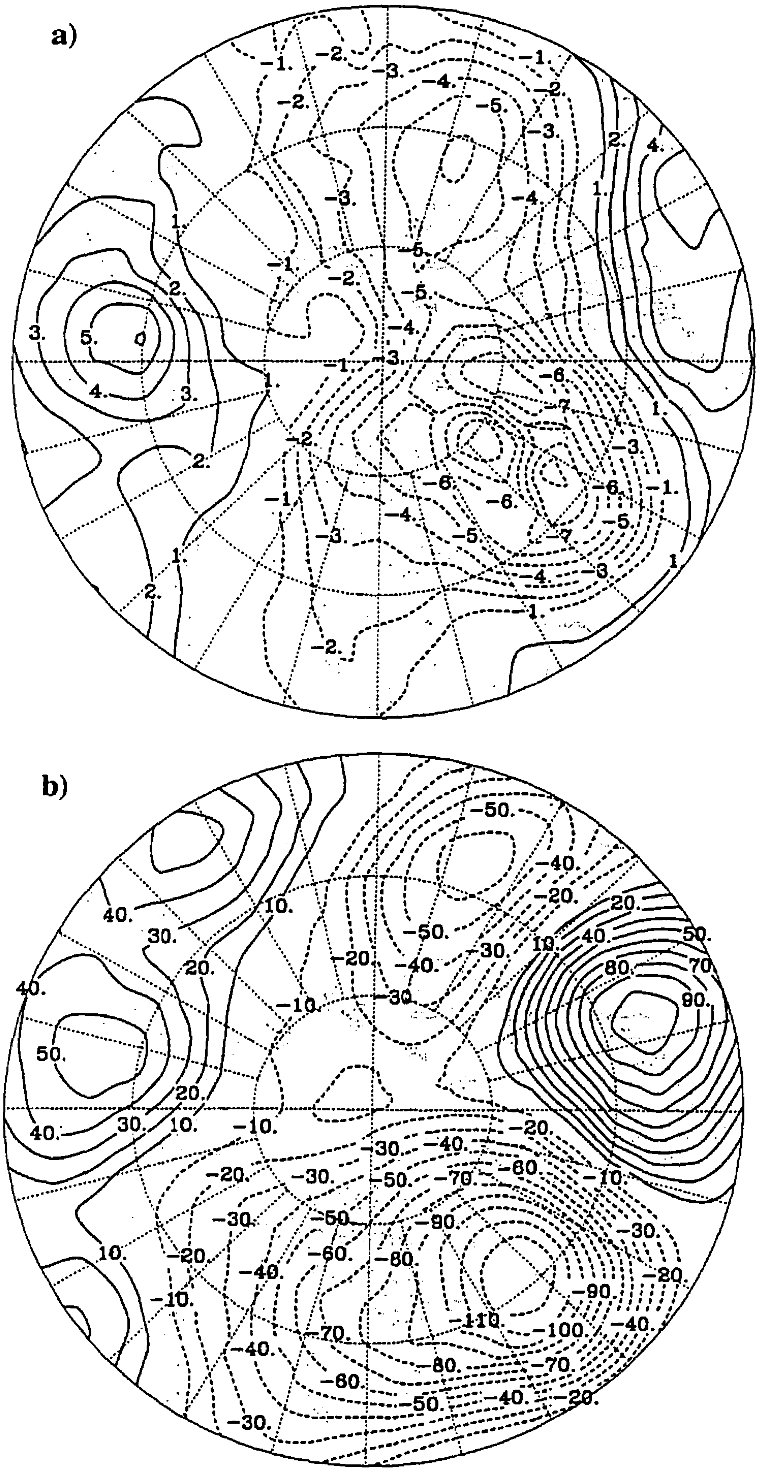

Figure 4.3 As in Figure 4.2, but for differences between 1966-70 and 1971-74.

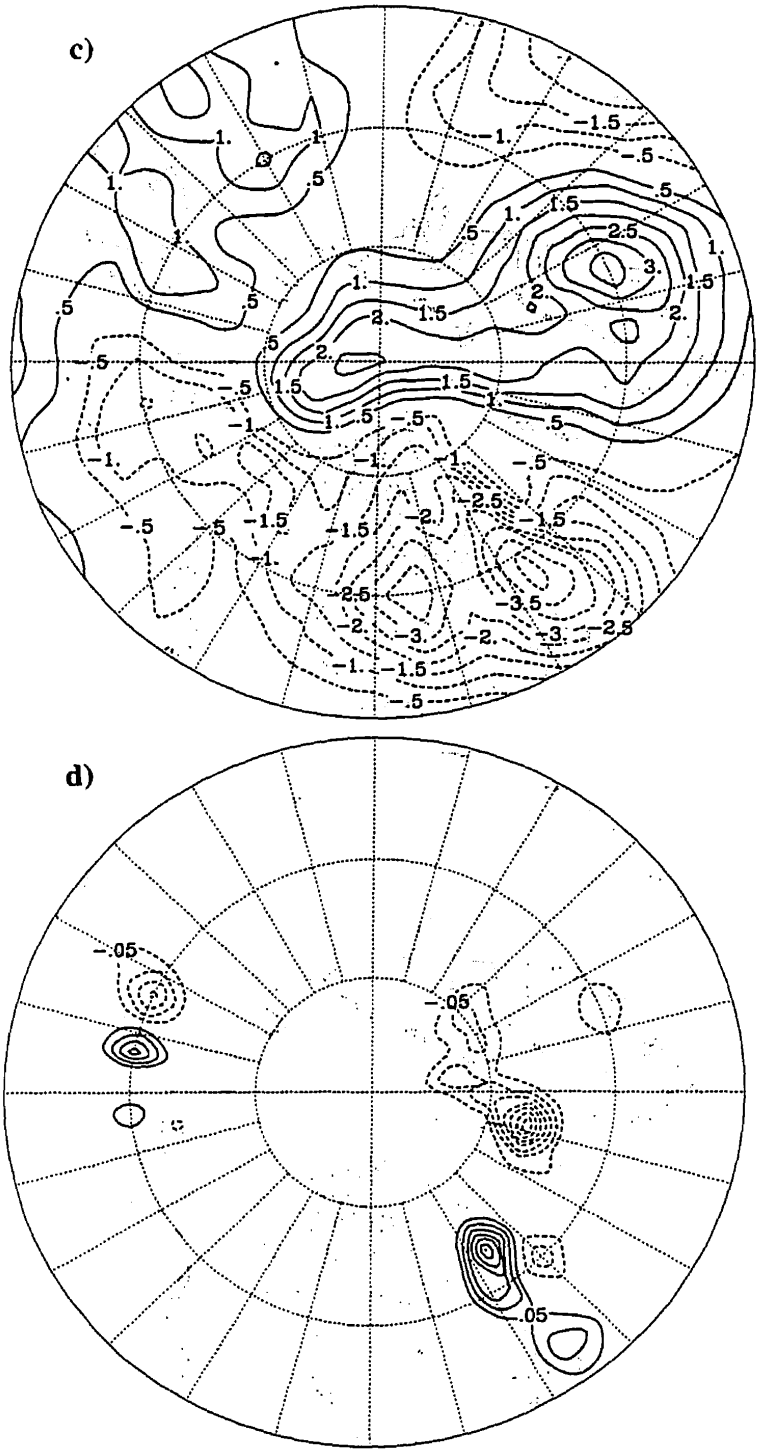

Figure 4.3 cont'd.

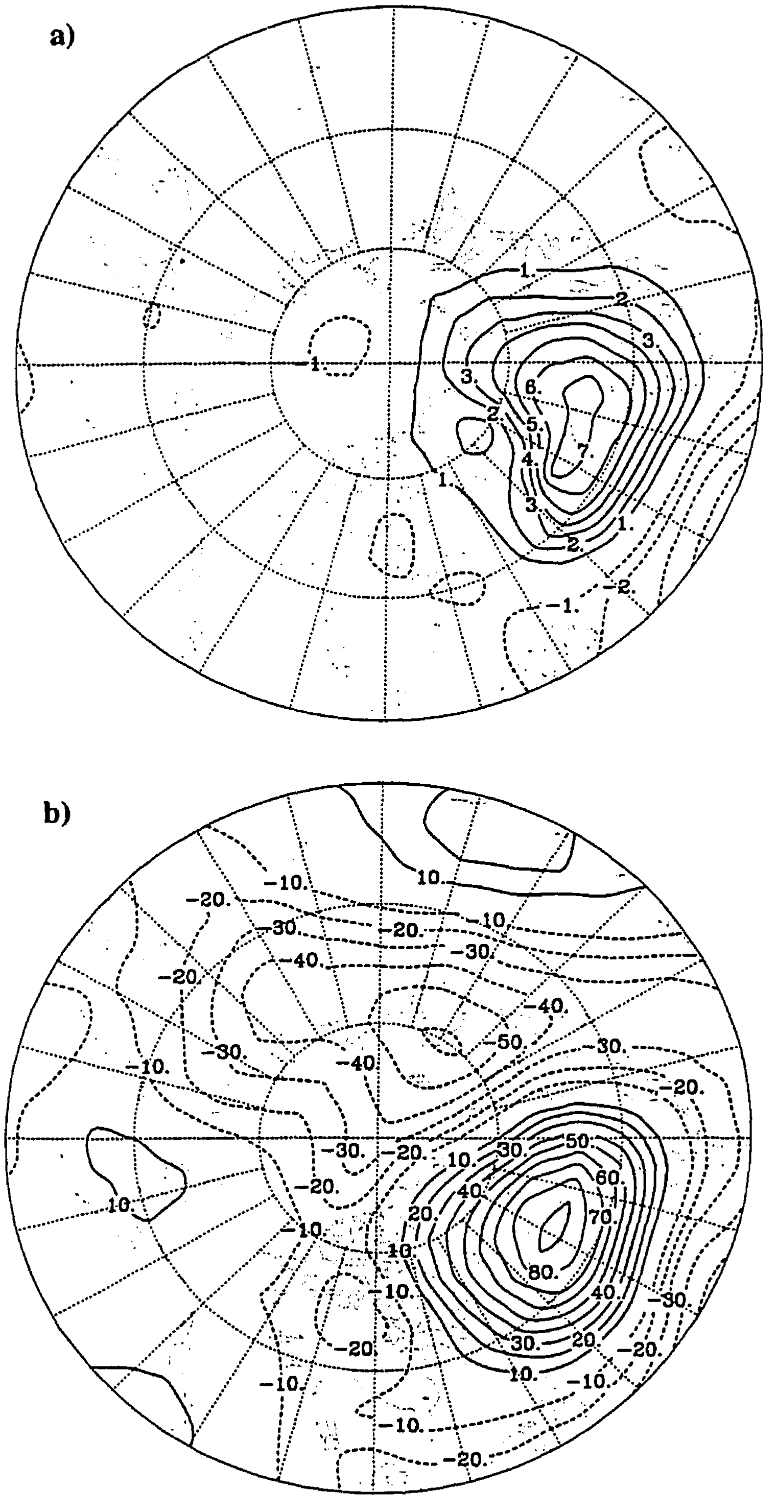

Figure 4.4 Mean anomalies for the period 1963-66 for a) SLP (in hPa), b) 500 Z (in m), c) 850 T (in °C) and d) sea ice concentration (in tenths).

c)

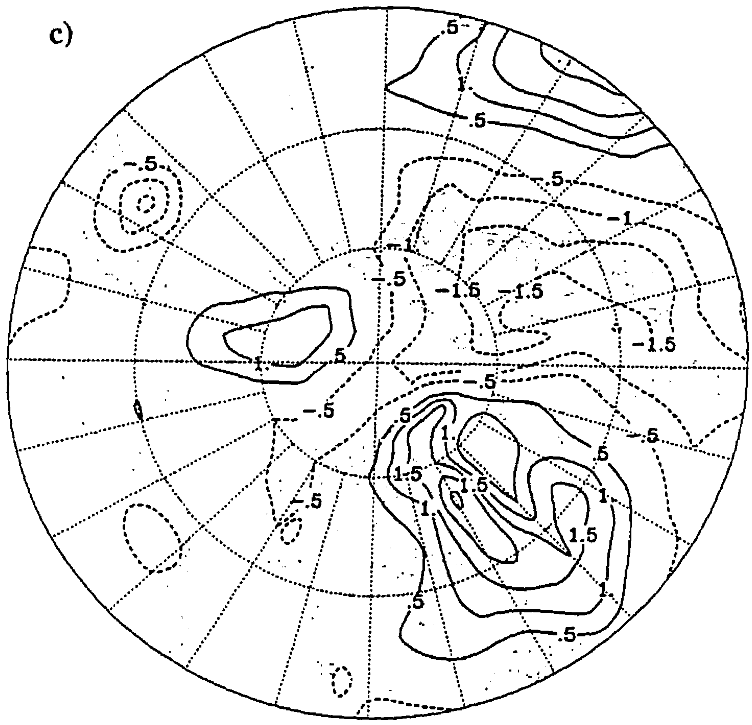

d)

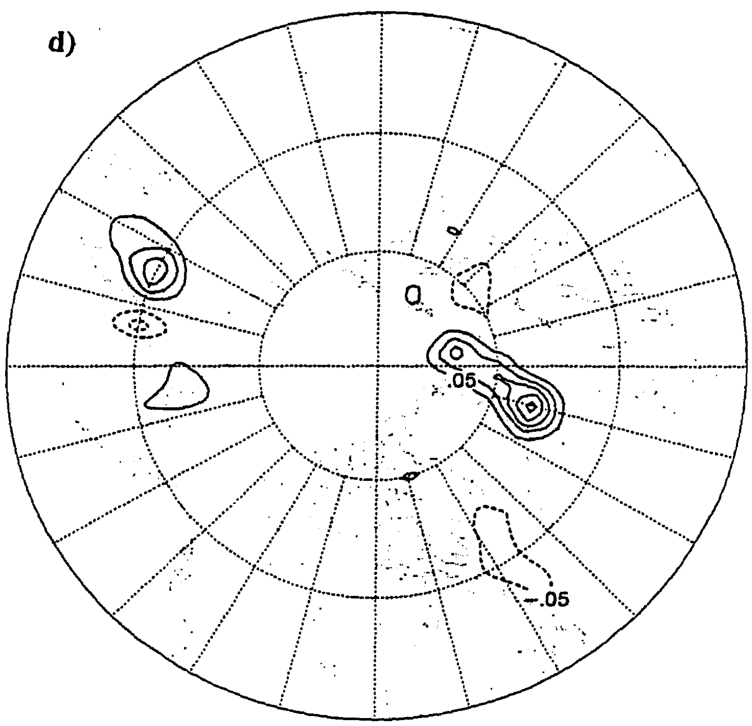

Figure 4.4 cont'd

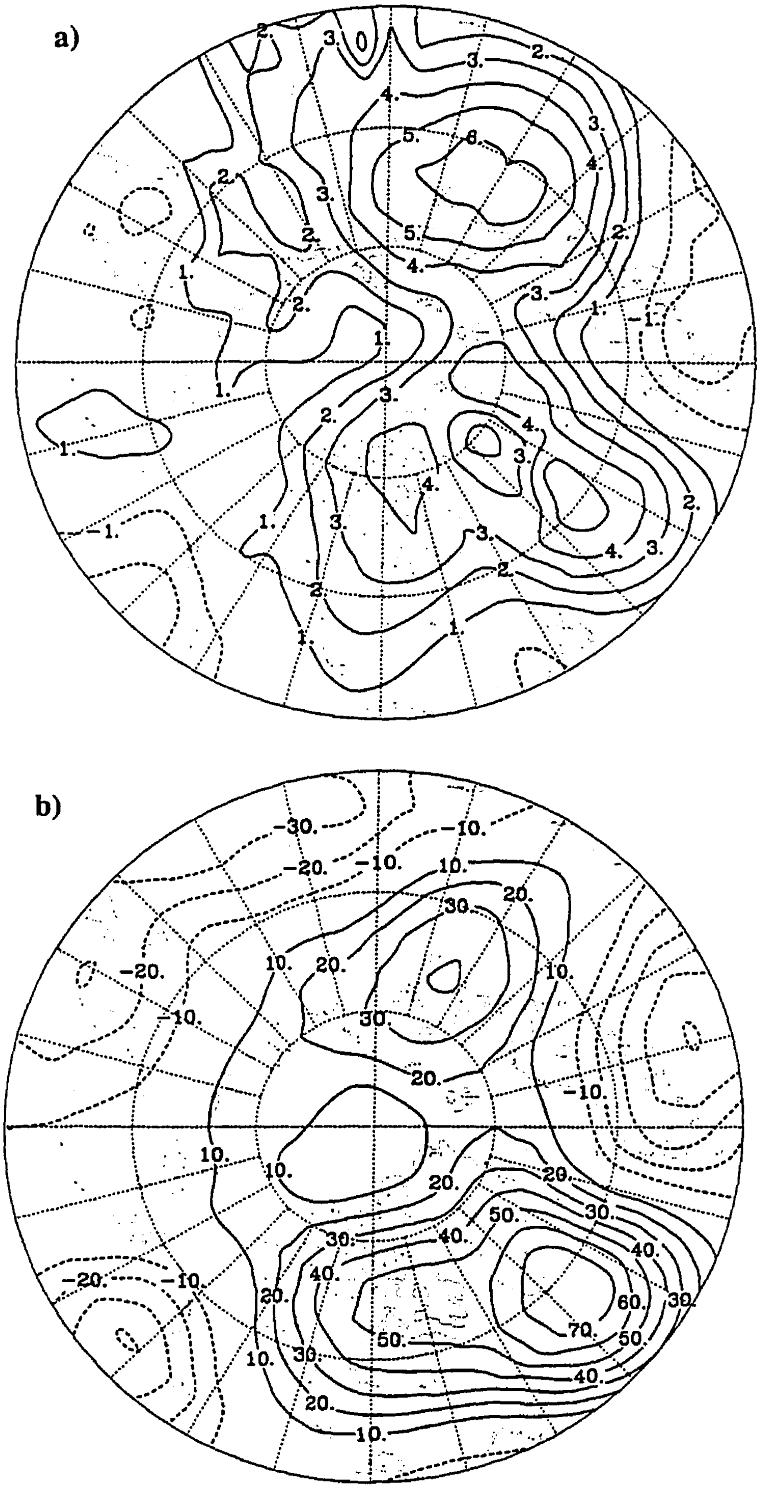

Figure 4.5 As in Figure 4.4, but for the period 1967-70.

c)

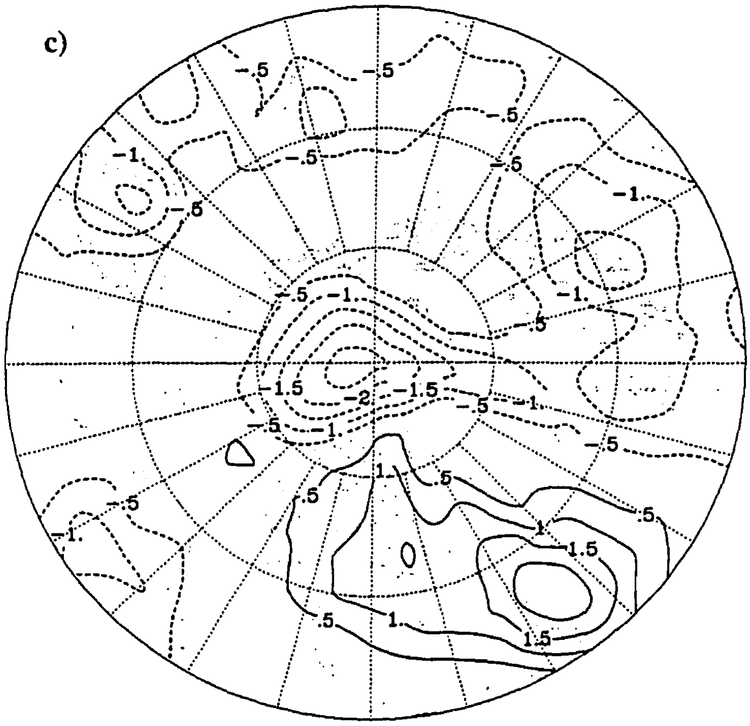

d)

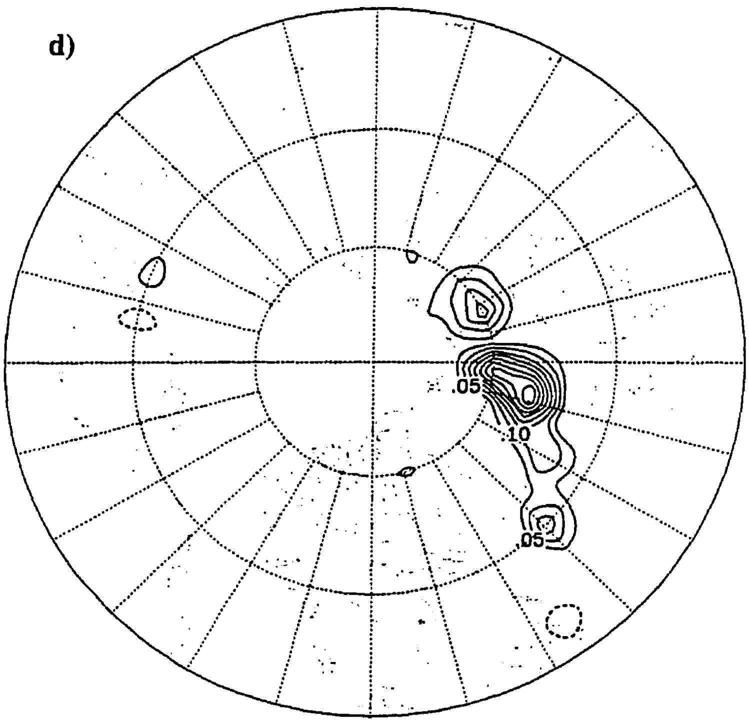

Figure 4.5 cont'd.

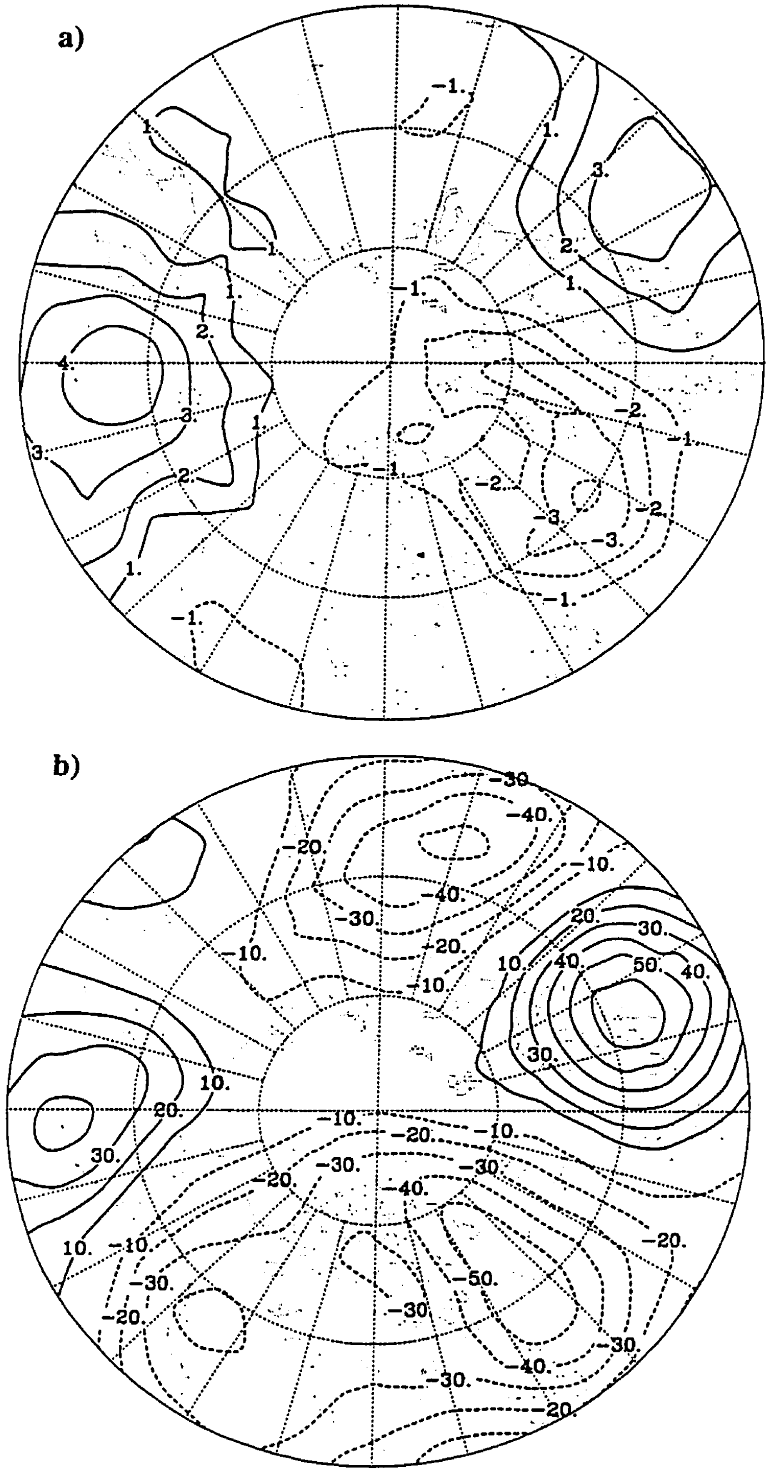

Figure 4.6 As in Figure 4.4, but for the period 1971-74.

c)

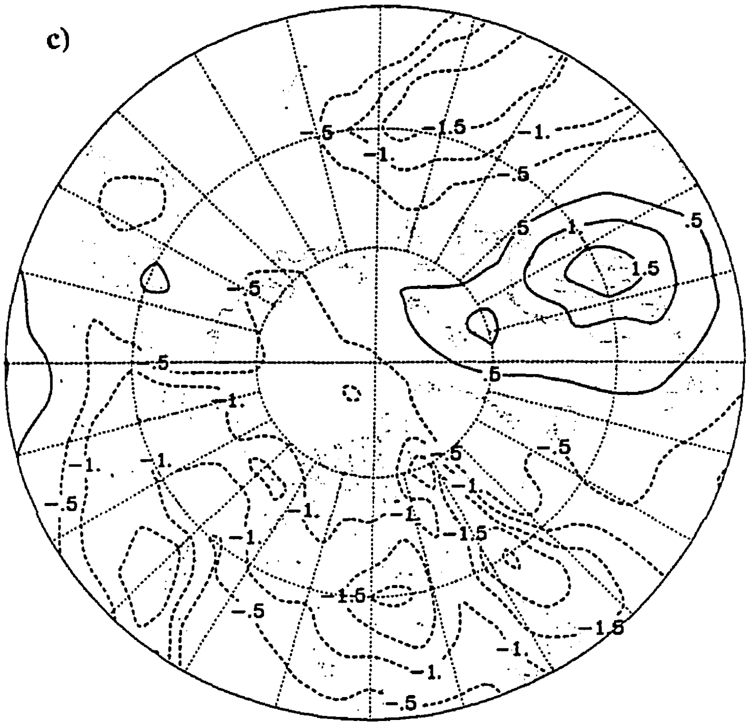

d)

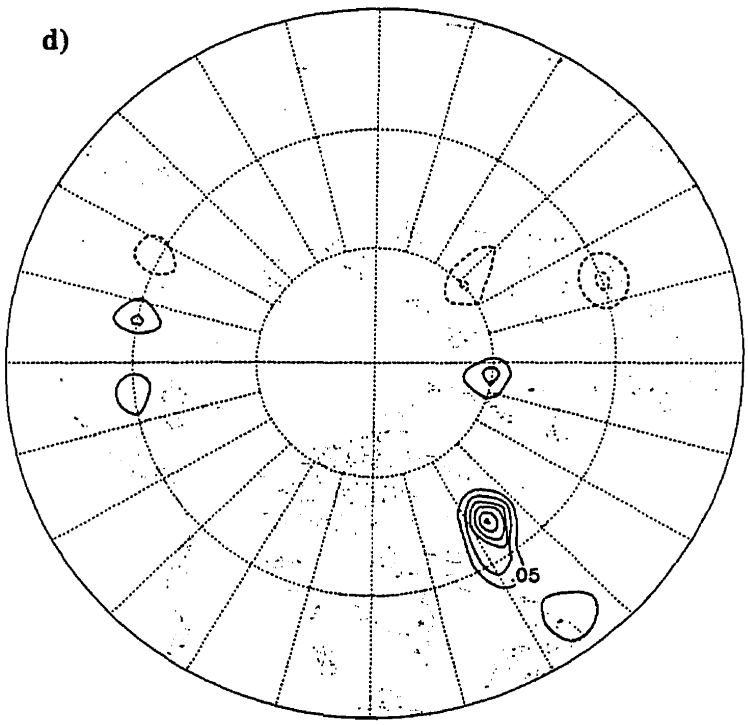

Figure 4.6 cont'd.

23.1%

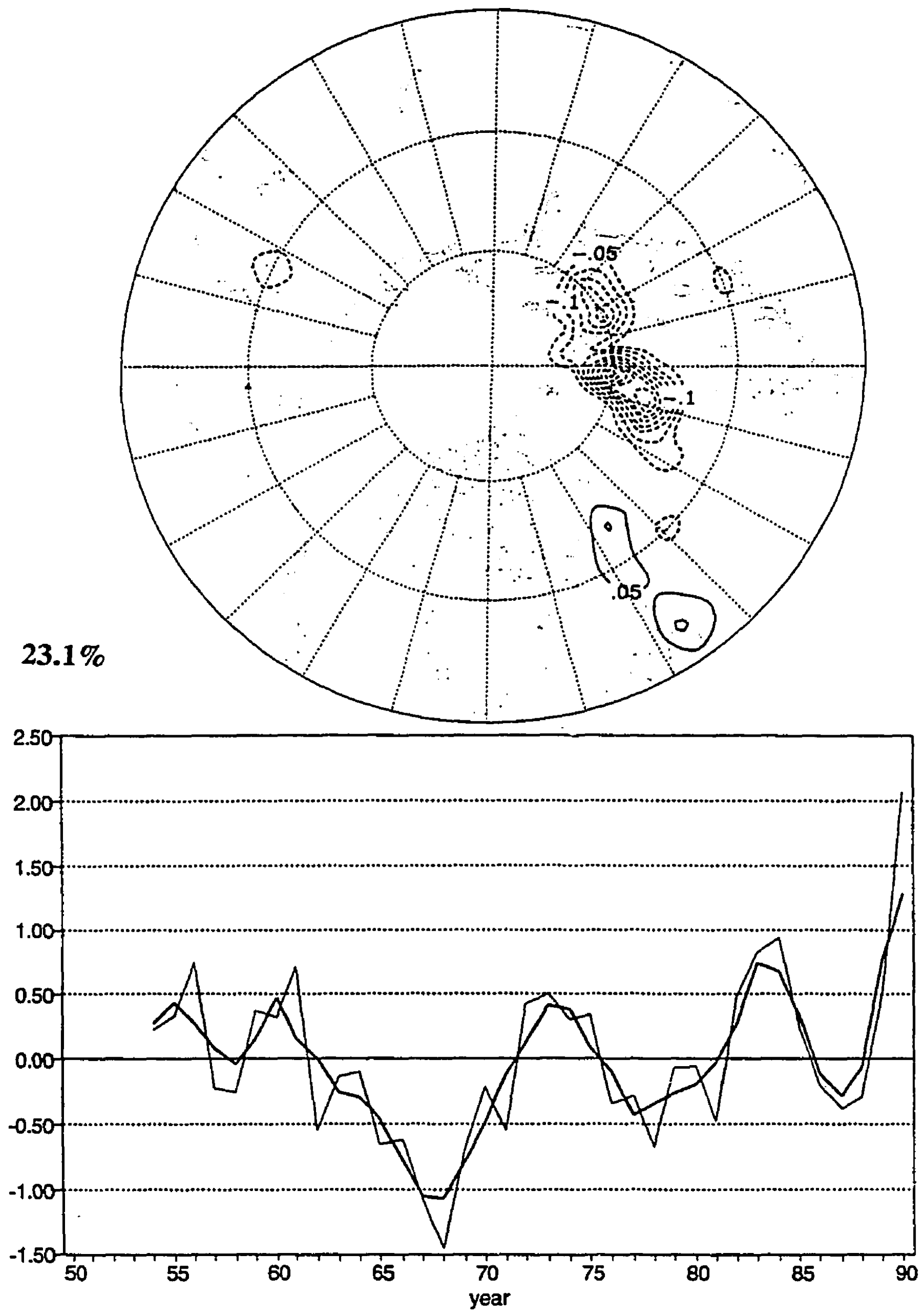

Figure 4.7 Spatial structure (top) and time series (bottom) of EOF 1 of winter sea ice concentration. Thick line in time series represents three year running mean.

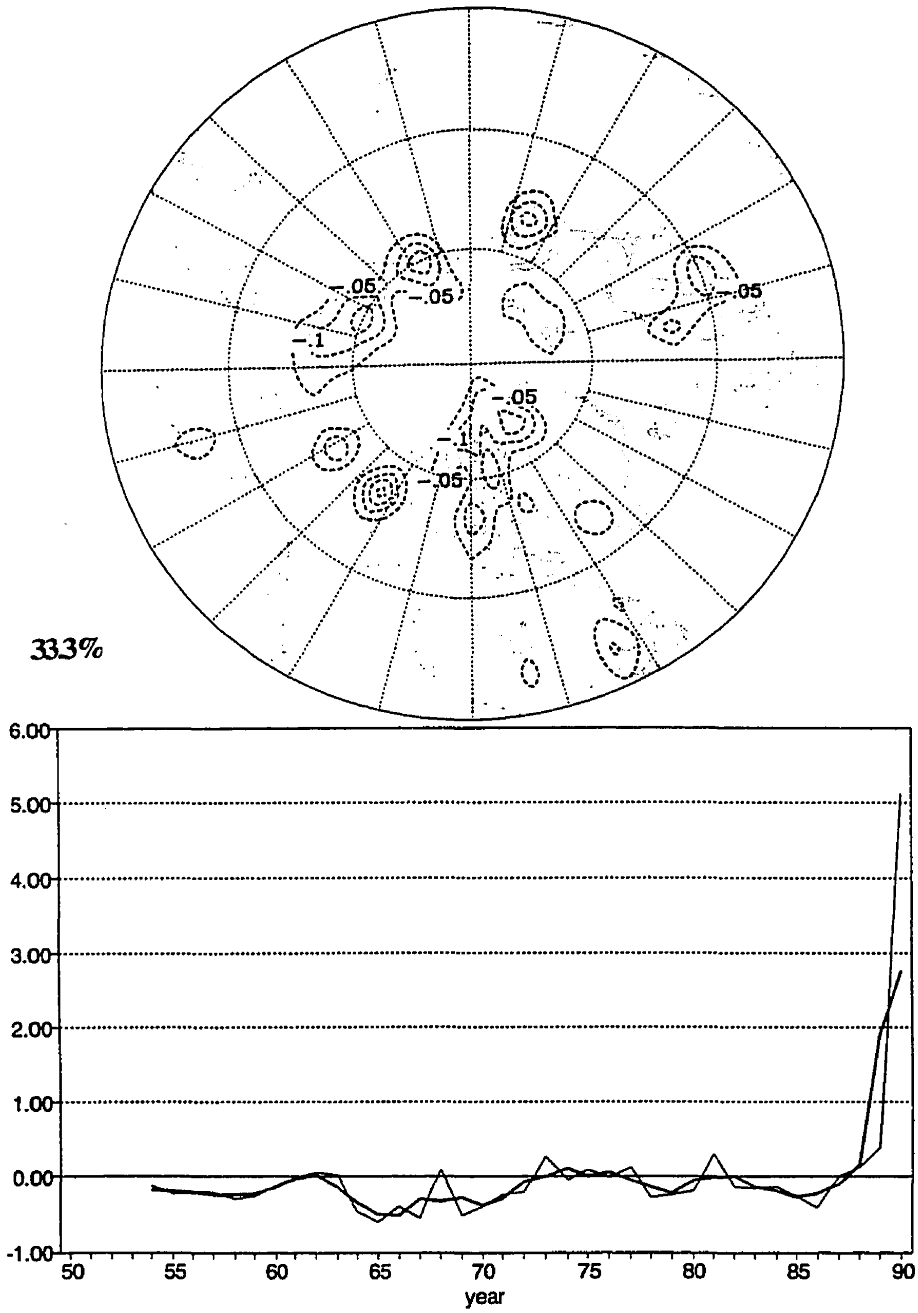

Figure 4.8 As in Figure 4.7, but for EOF 1 of summer sea ice concentration for the period 1954-1990.

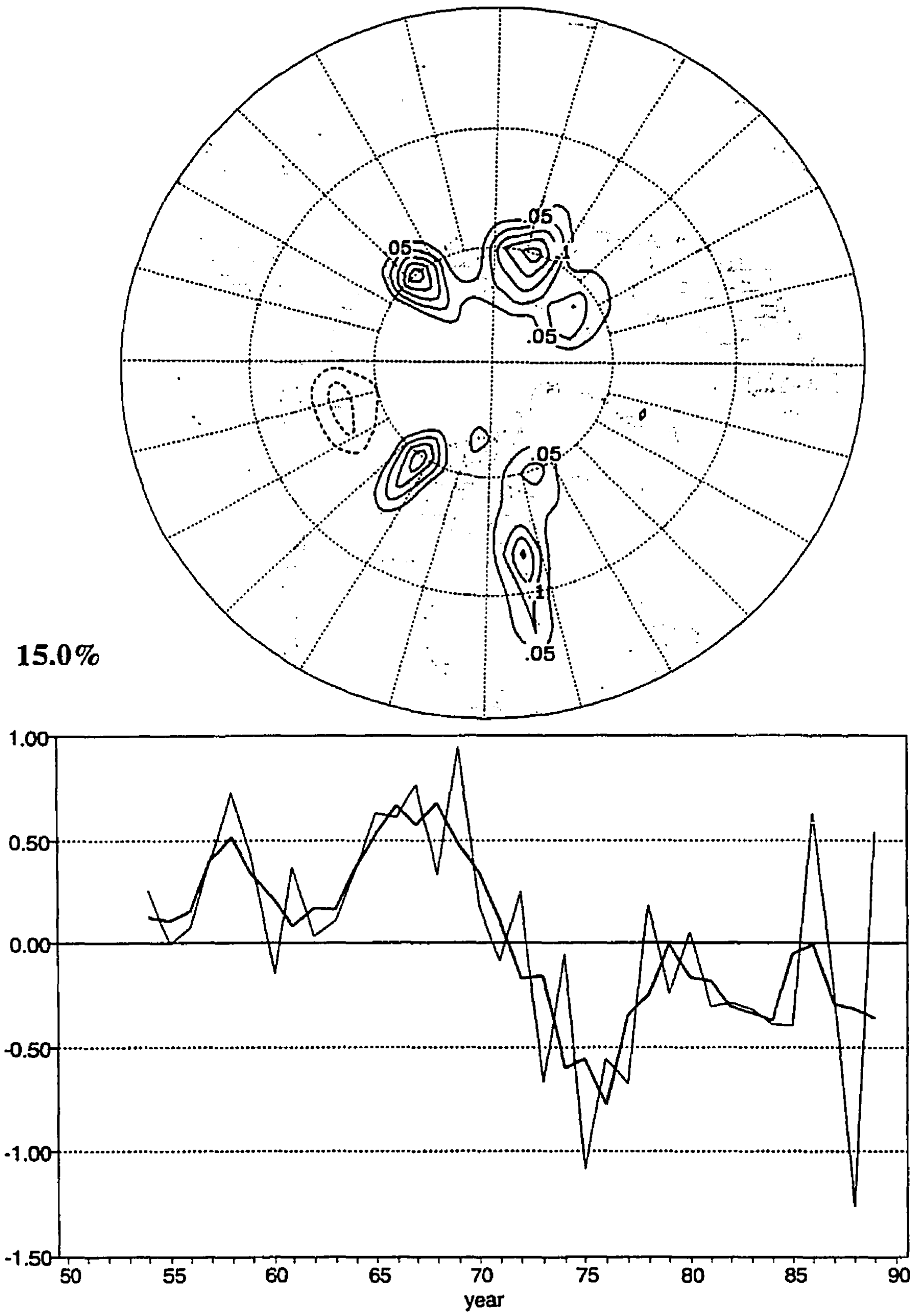

Figure 4.9 As in Figure 4.7, but for EOF 1 of summer sea ice concentration for the period 1954-1989.

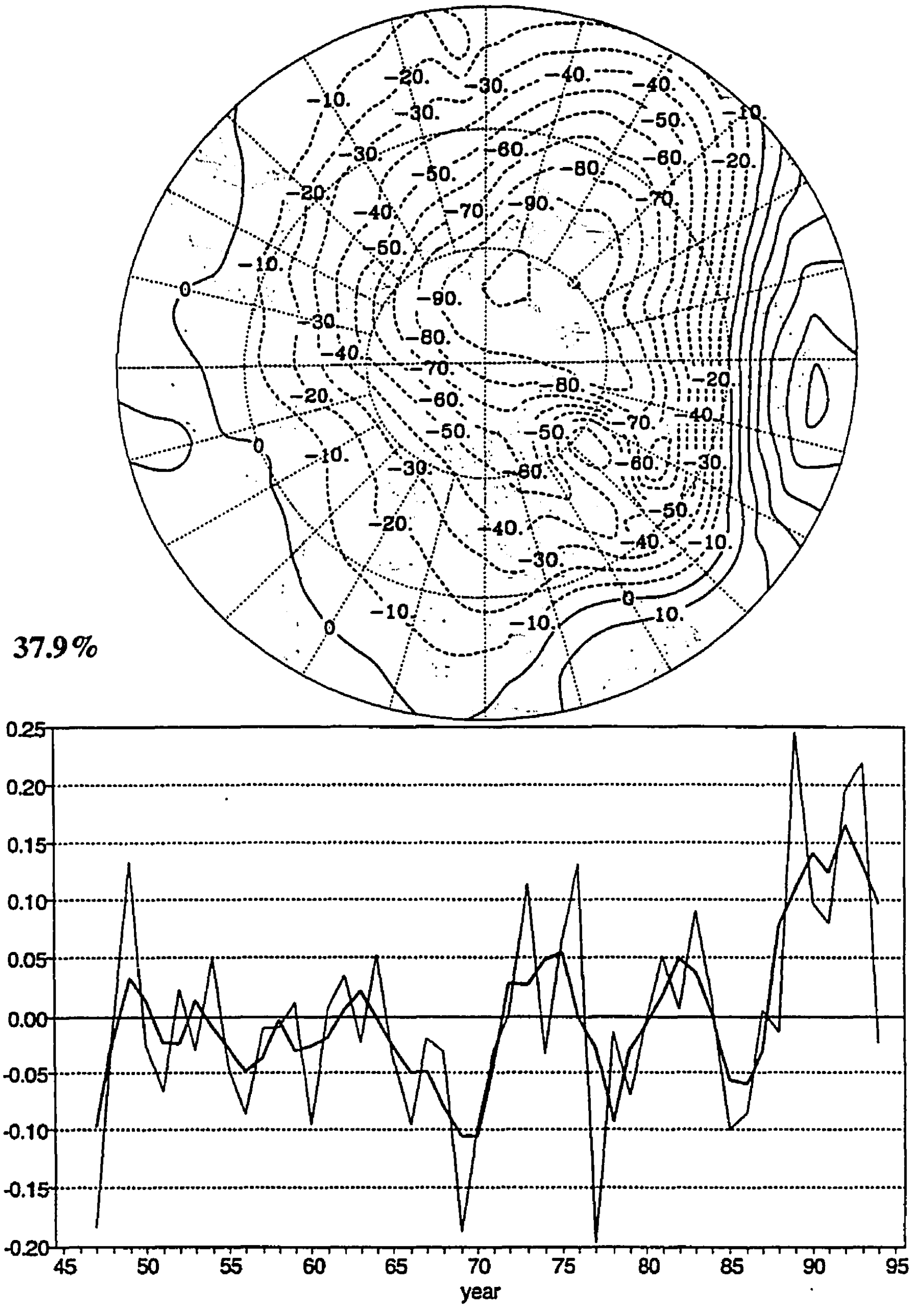

Figure 4.10 As in Figure 4.7, but for EOF 1 of winter SLP.

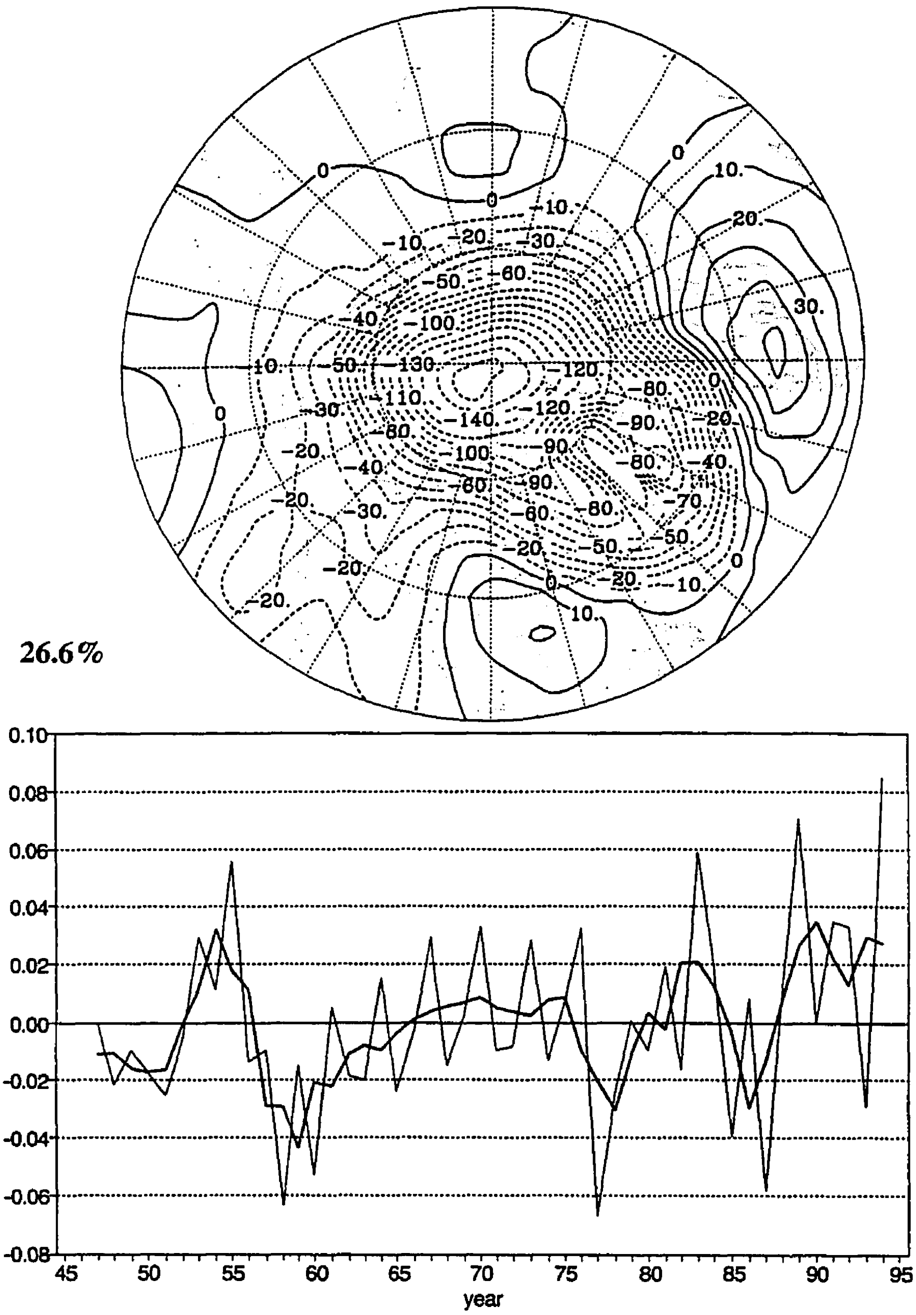

Figure 4.11 As in Figure 4.7, but for EOF 1 of summer SLP.

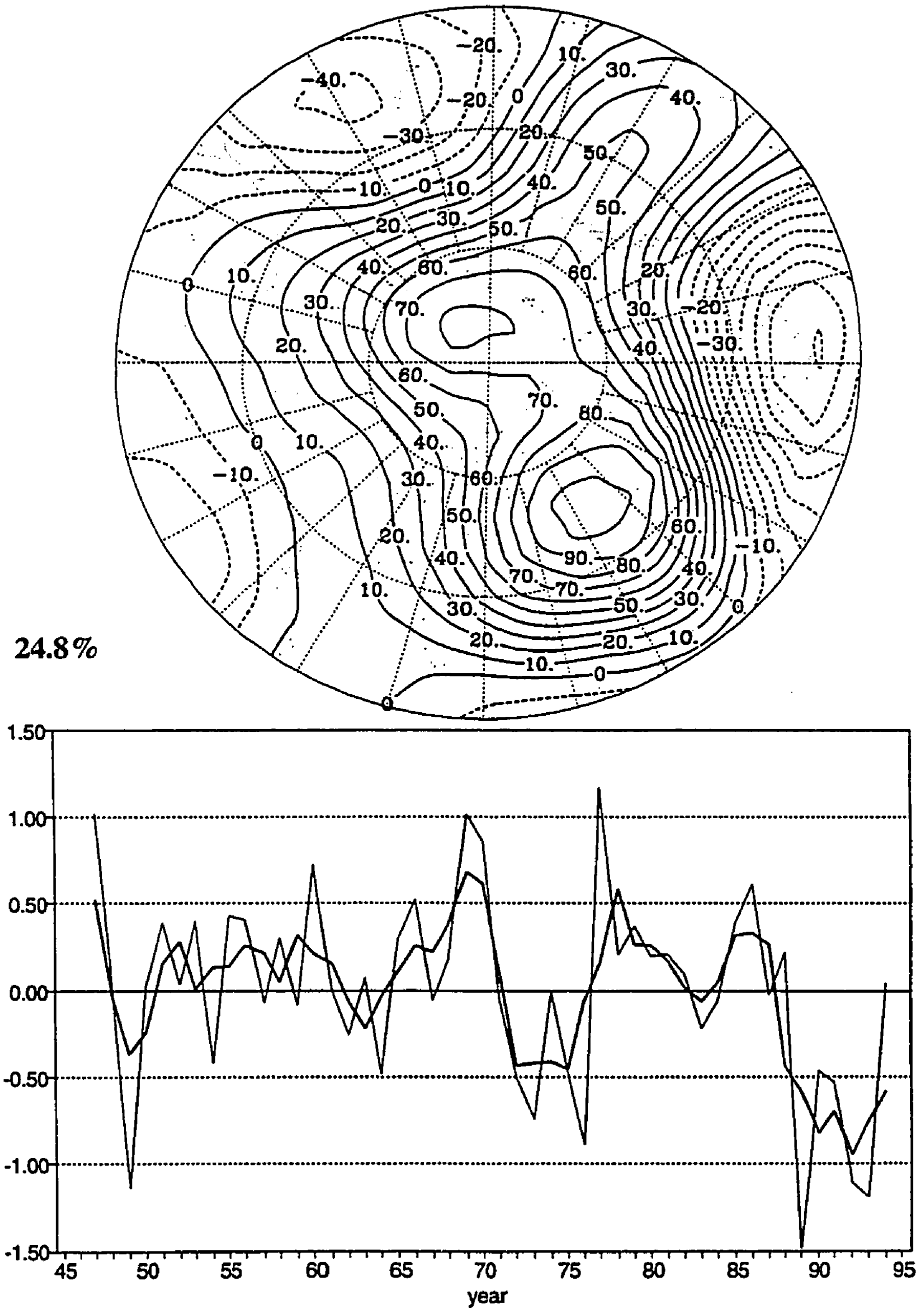

Figure 4.12 As in Figure 4.7, but for EOF 1 of winter 500 Z.

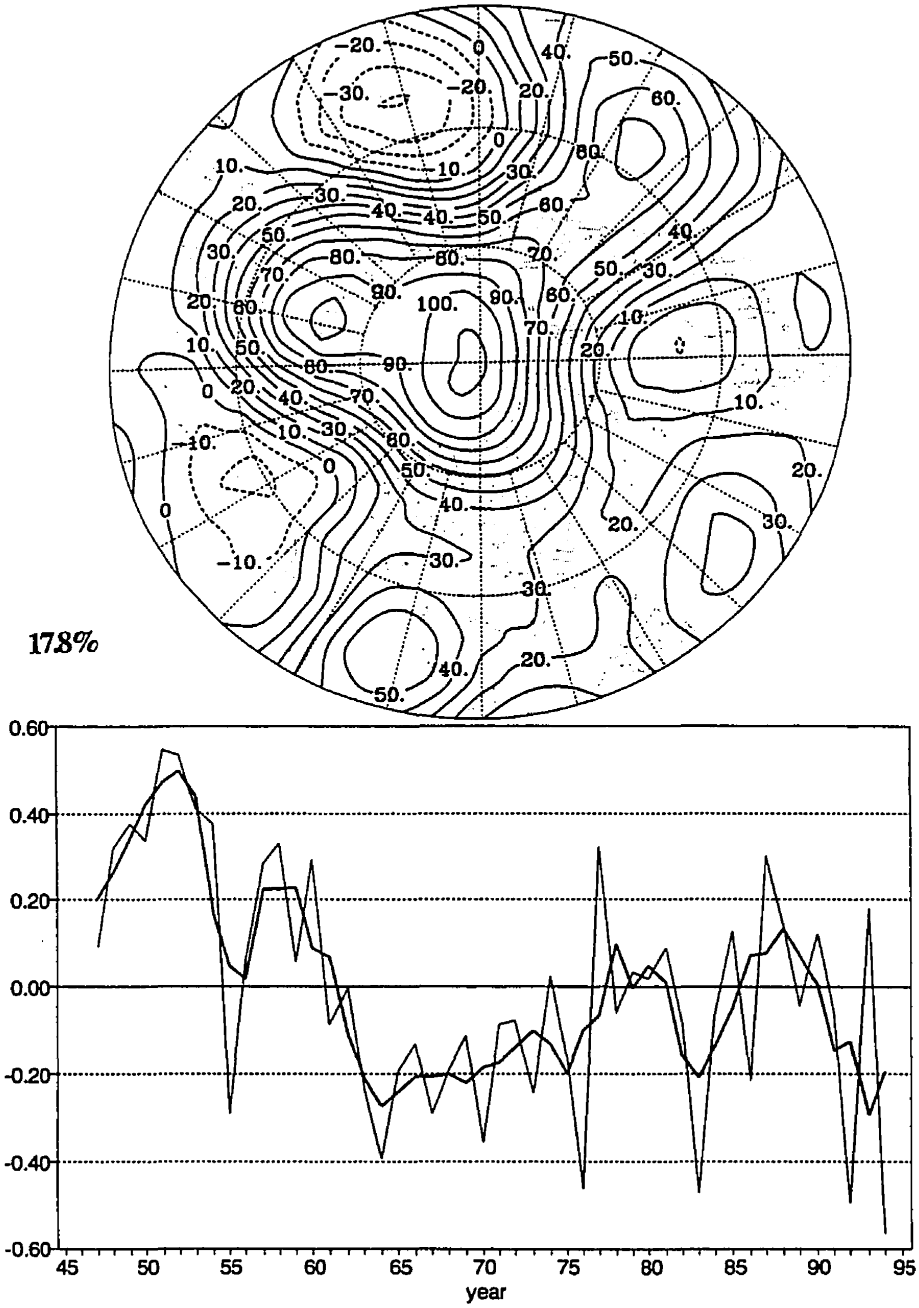

Figure 4.13 As in Figure 4.7, but for EOF 1 of summer 500 Z.

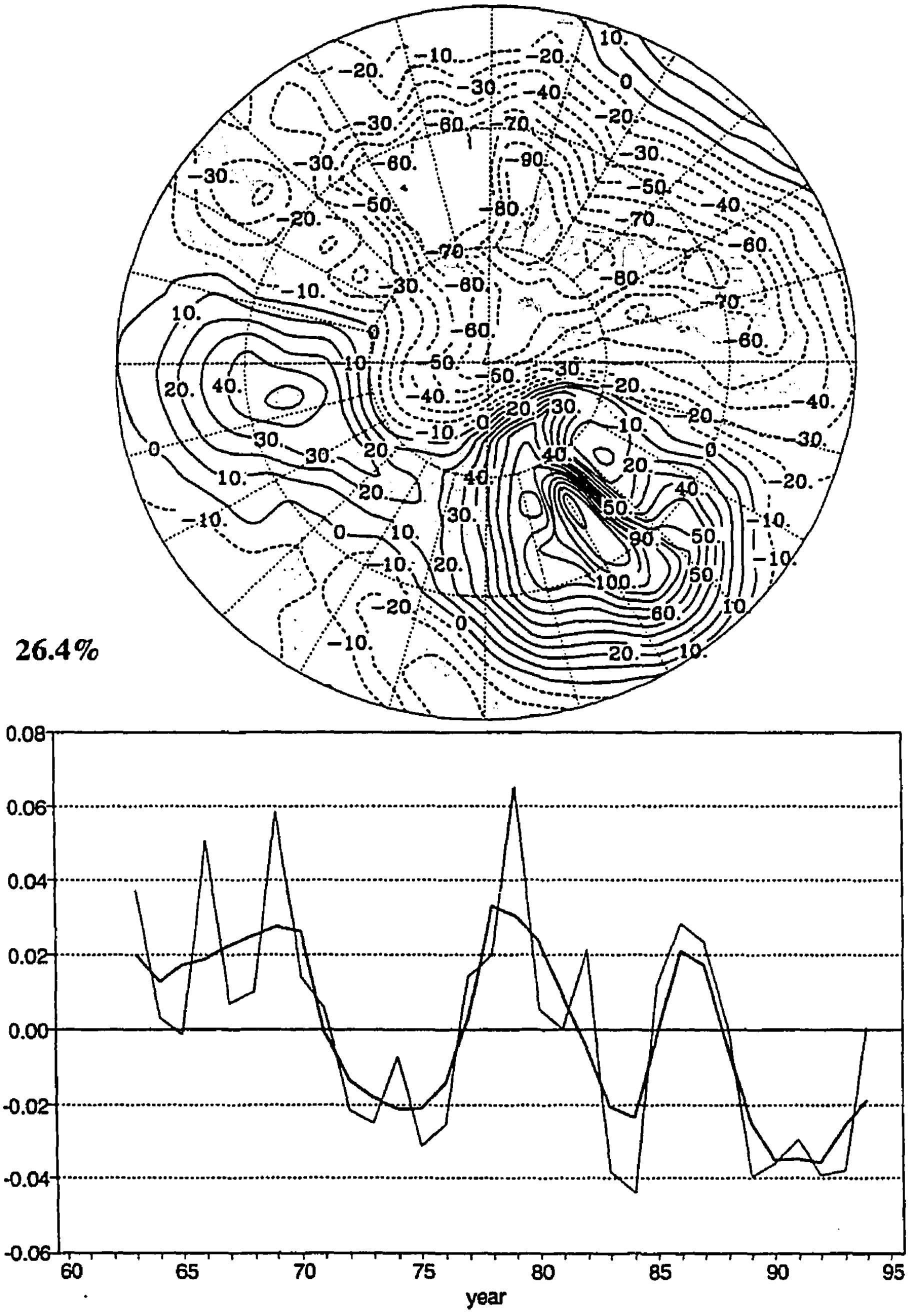

Figure 4.14 As in Figure 4.7, but for EOF 1 of winter 850 T.

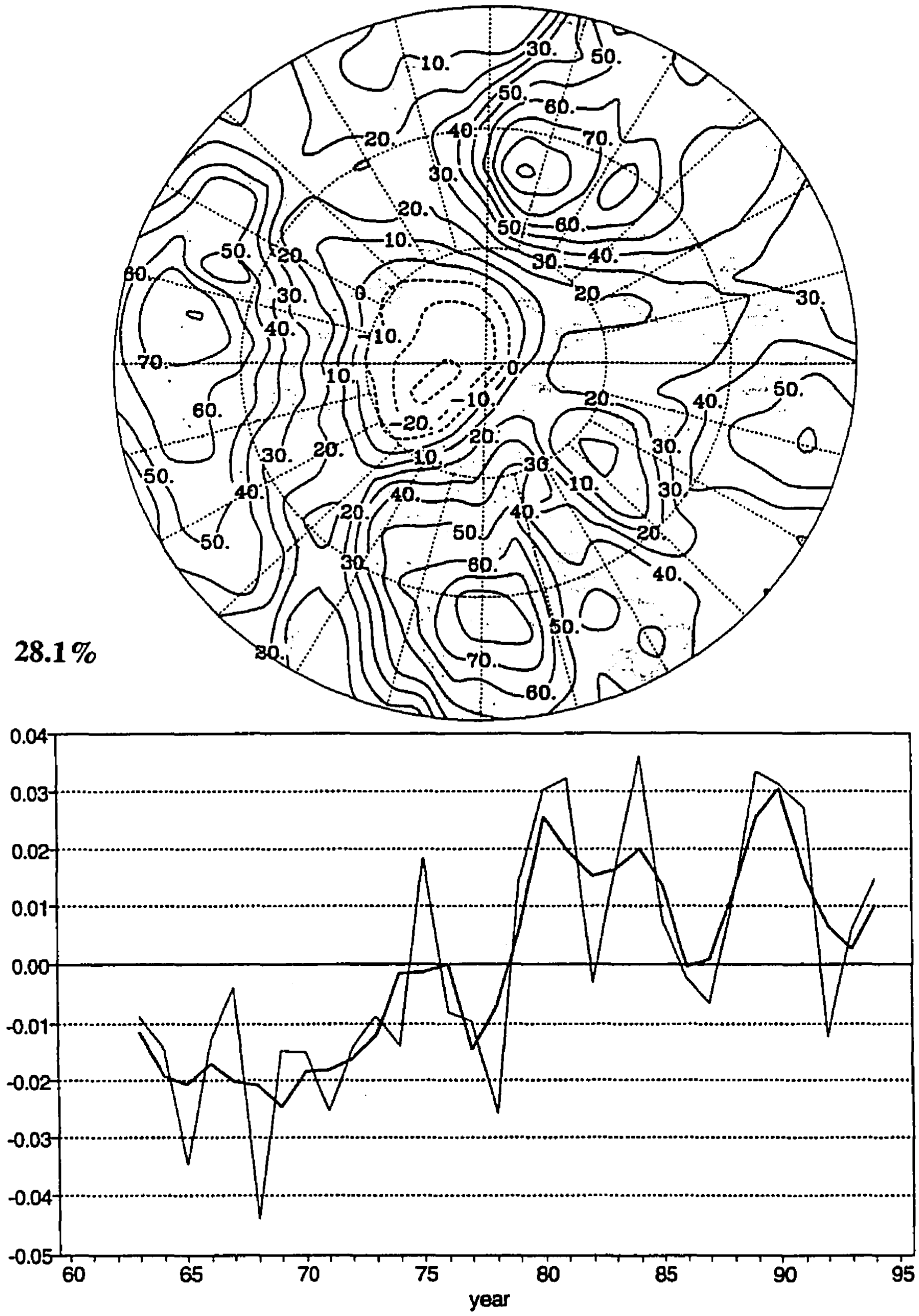

Figure 4.15 As in Figure 4.7, but for EOF 1 of summer 850 T.

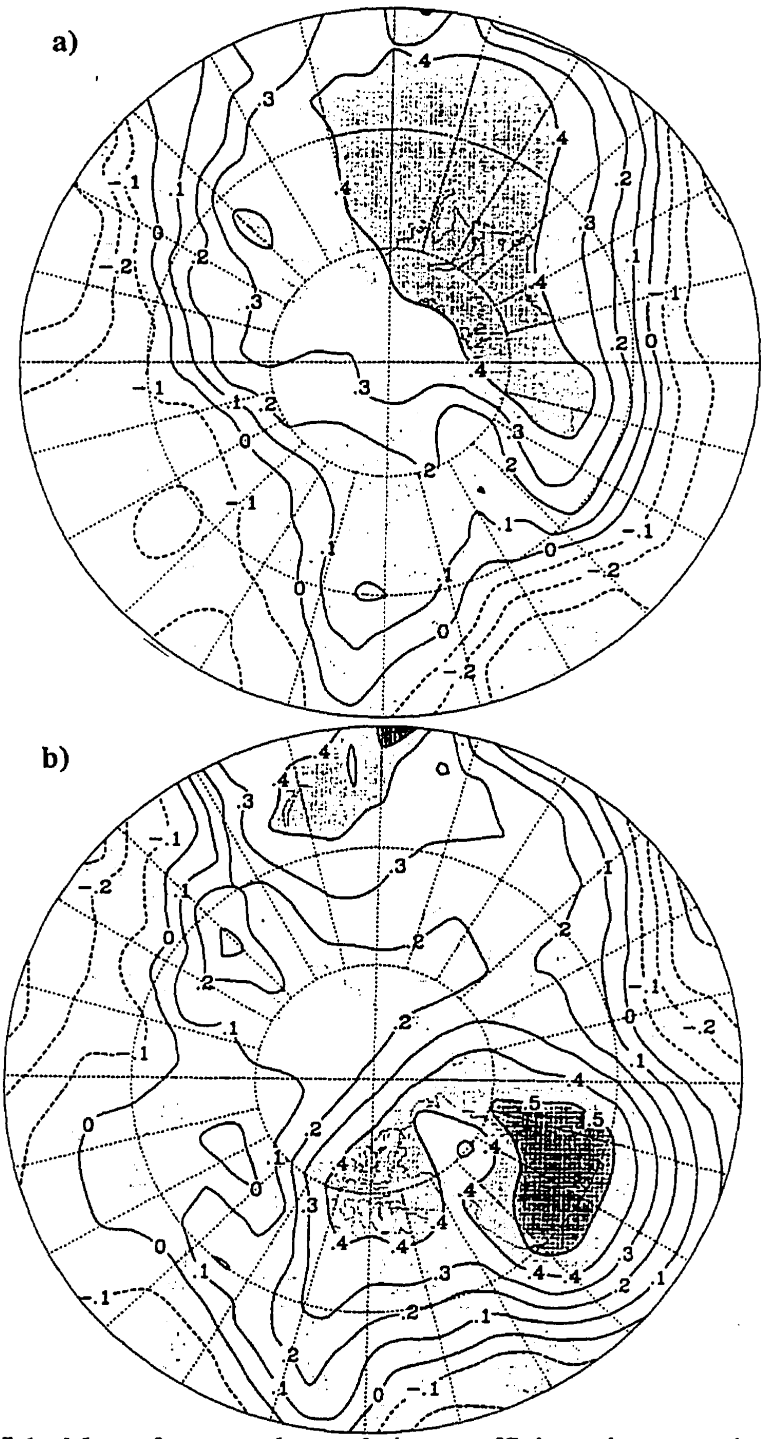

Figure 5.1 Map of temporal correlation coefficients between the time series of EOF 1 of winter sea ice concentration (see Figure 4.7) and winter SLP anomalies for the period 1947-1994 for a) lag of -1 (atmosphere leading ice by one year), b) zero lag and c) lag of +1 (ice leading atmosphere by one year). Lightly shaded areas represent correlations that are significant at the 95% level, dark shading represents areas of 99% significance.

c)

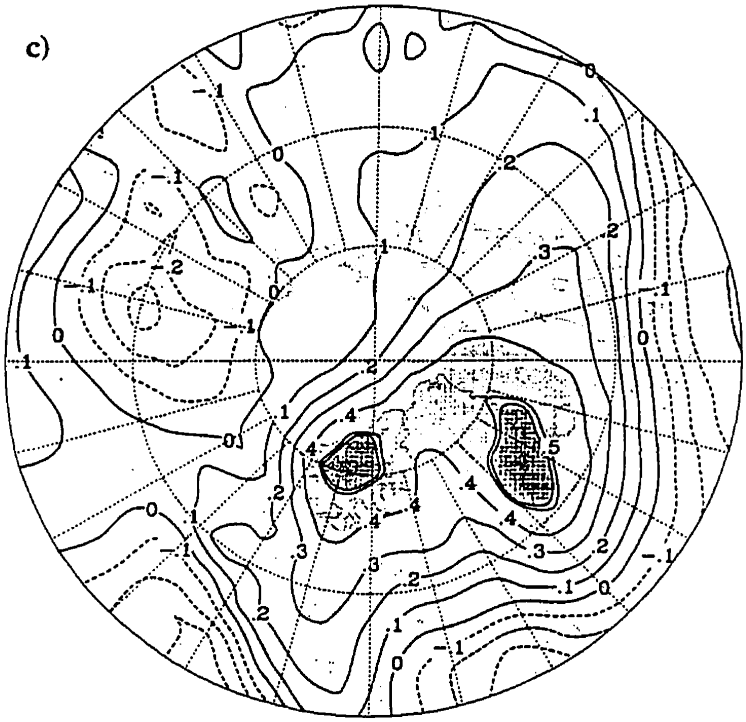

Figure 5.1 cont'd.

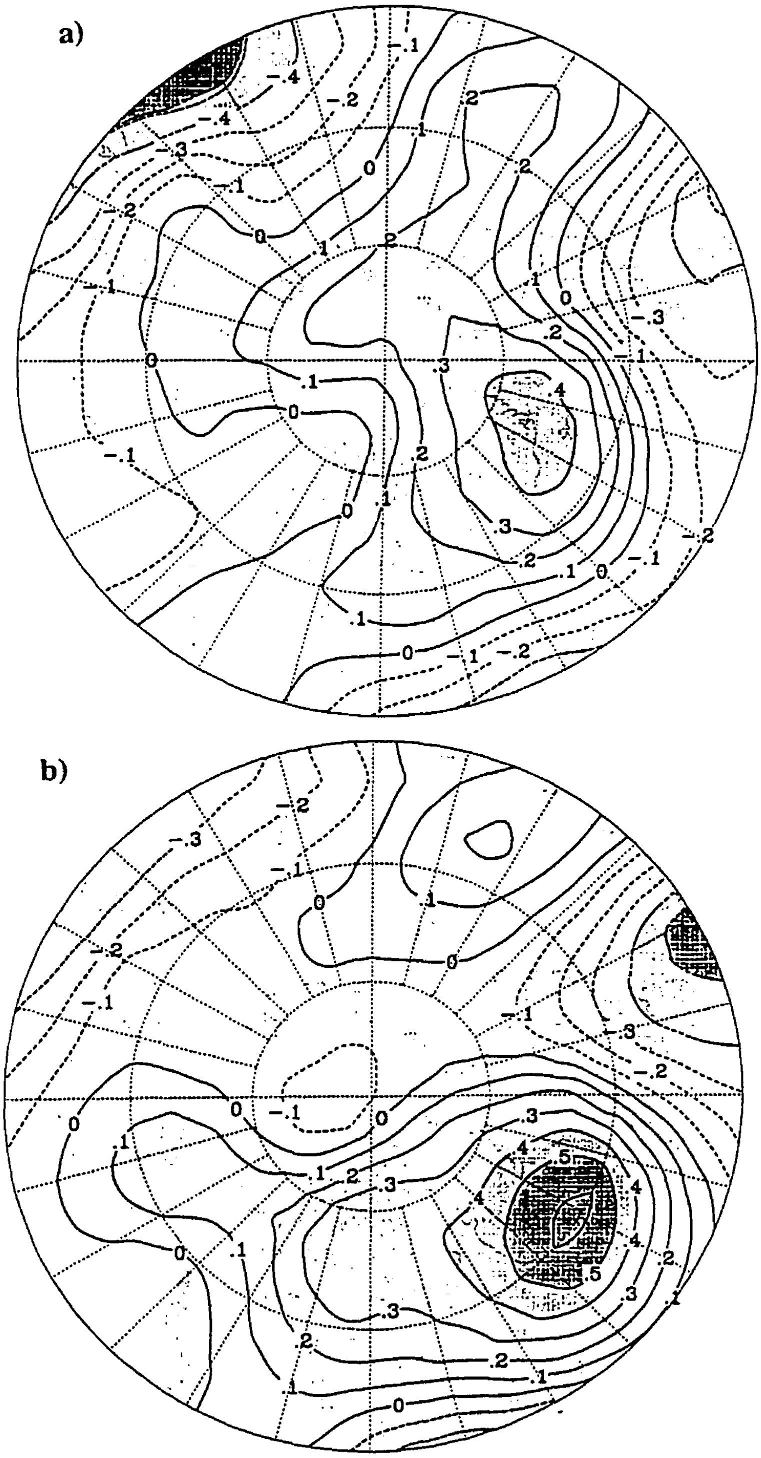

Figure 5.2 As in Figure 5.1, but for winter 500 Z.

c)

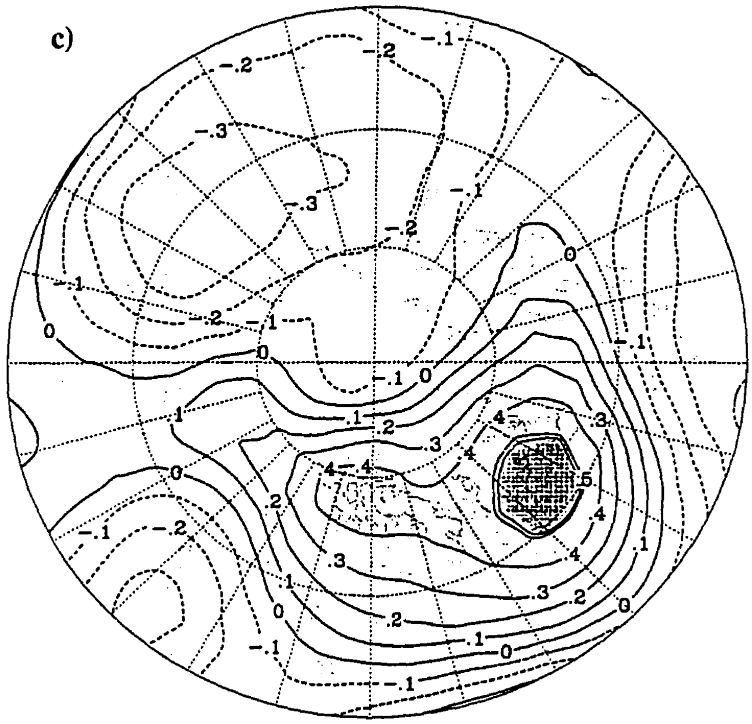

Figure 5.2 cont'd.

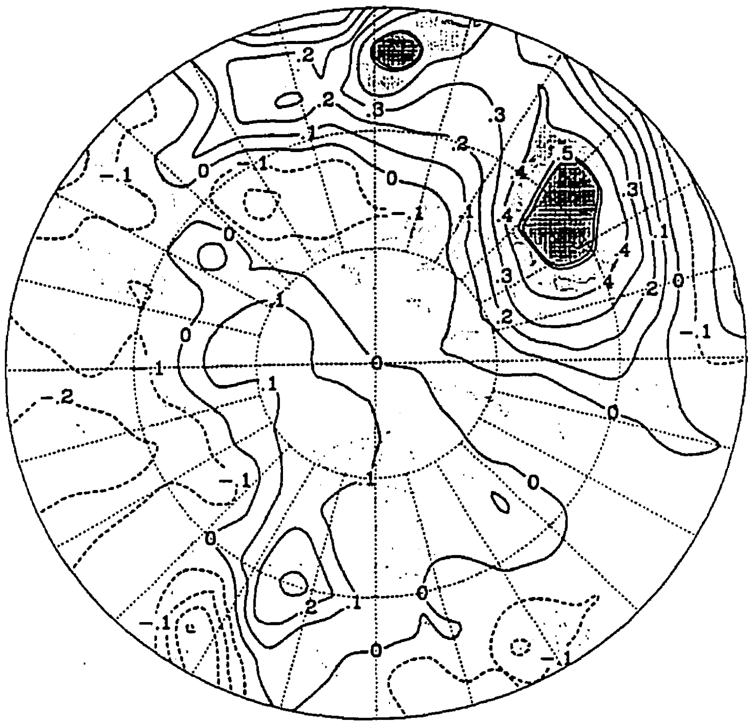

Figure 5.3 As in Figure 5.1, but for summer SLP at a lag of +1 1/2 years.

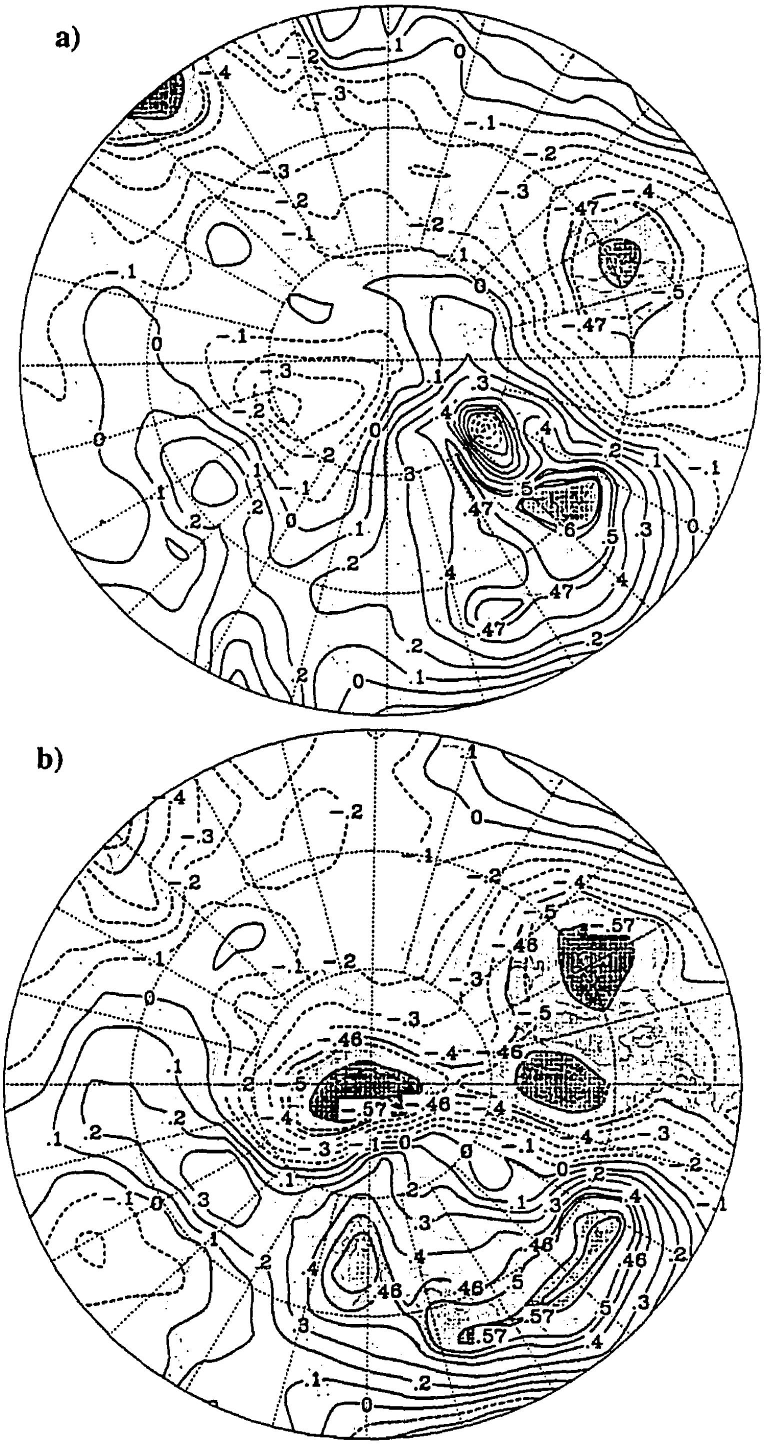

Figure 5.4 As in Figure 5.1, but for winter 850 T for the period 1963-1994.

c)

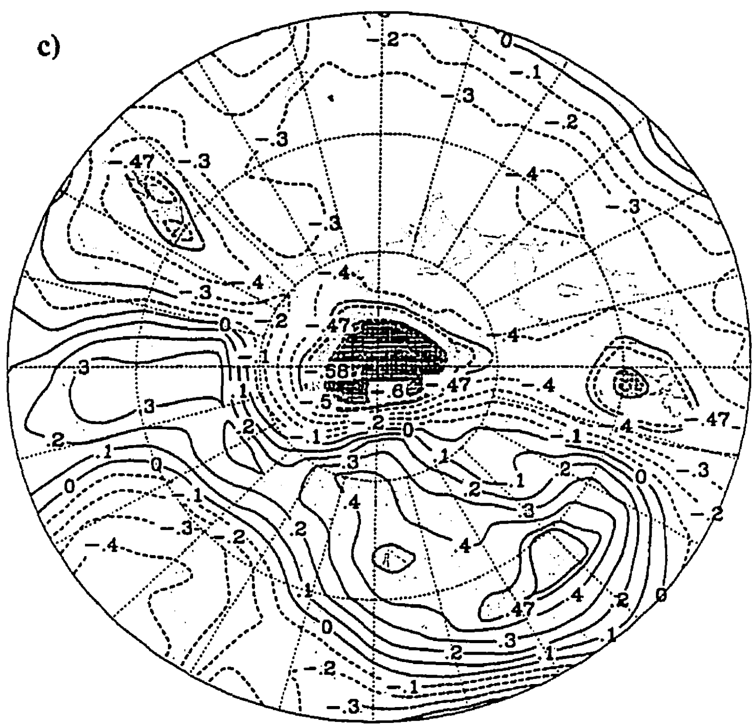

Figure 5.4 cont'd.

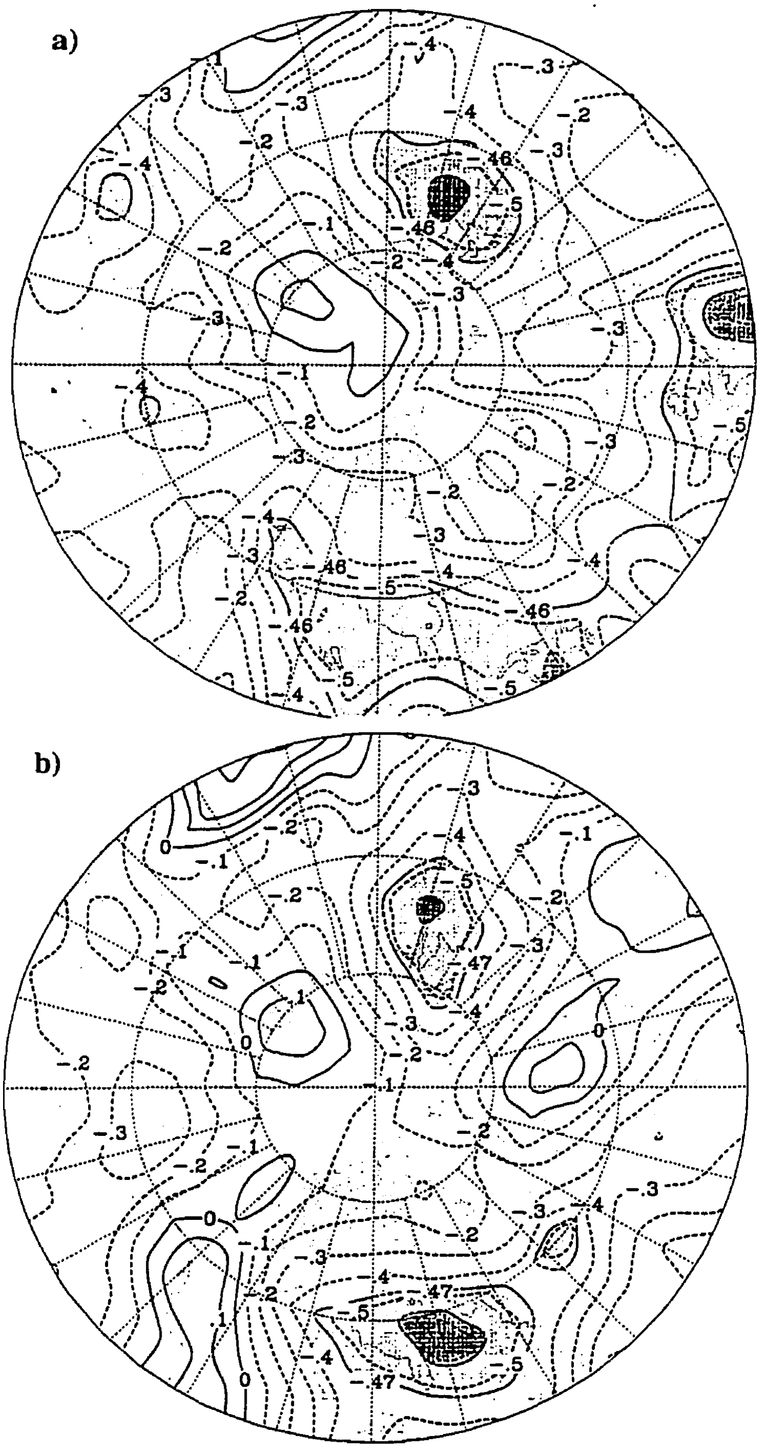

Figure 5.5 As in Figure 5.1, but for summer 850 T for the period 1963-1994 for a) lag of +1/2 and b) lag of +1 1/2.

a)

b)

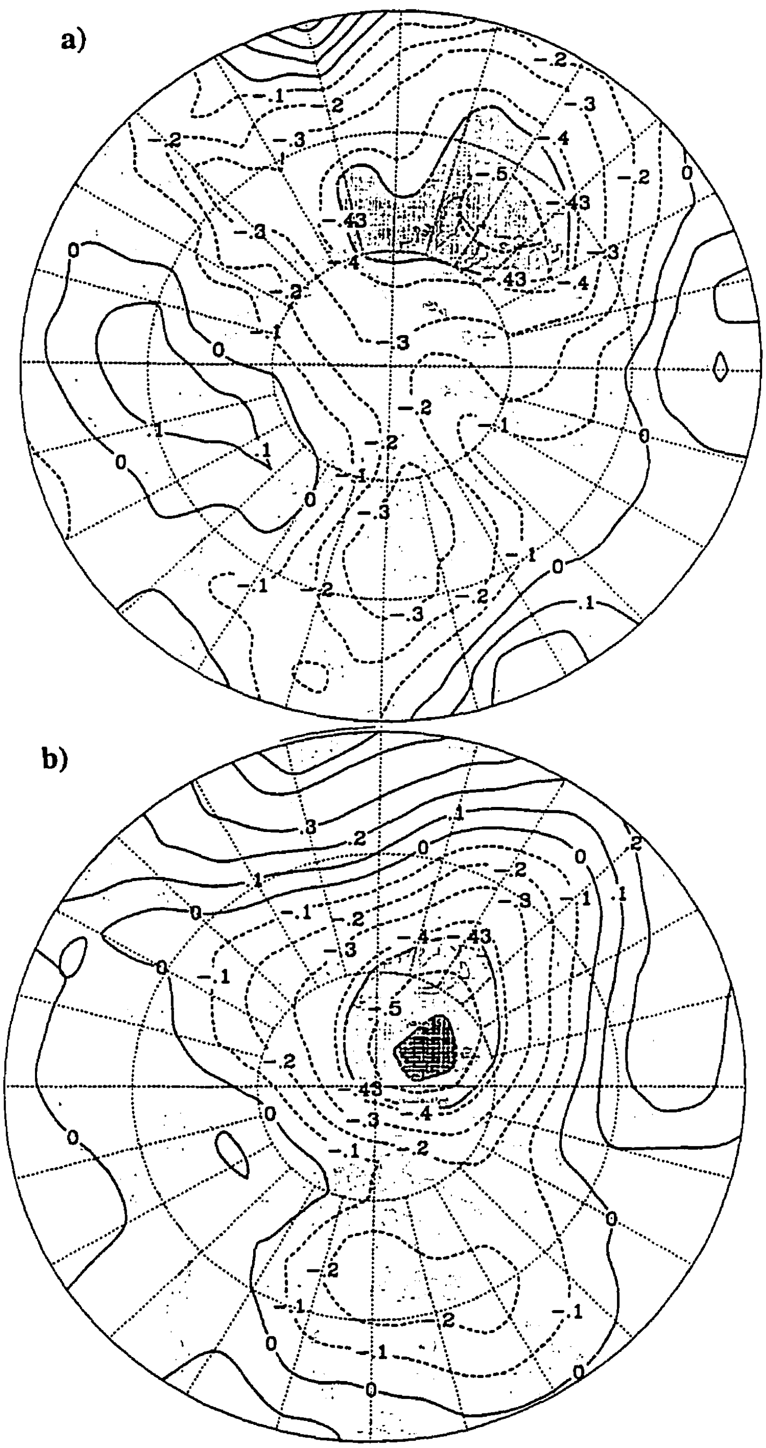

Figure 5.6 As in Figure 5.1, but for a) winter SLP, and b) winter 500 Z at lag -5.

a)

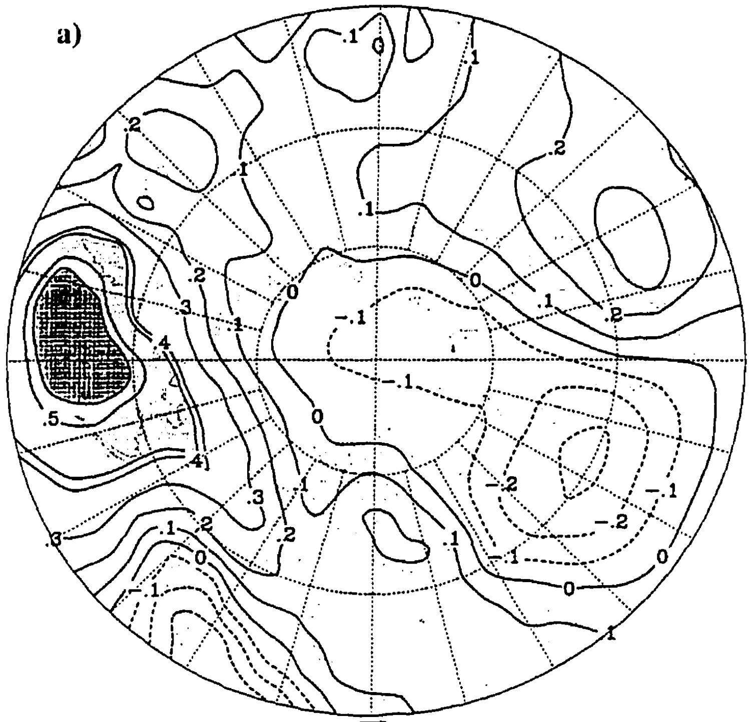

b)

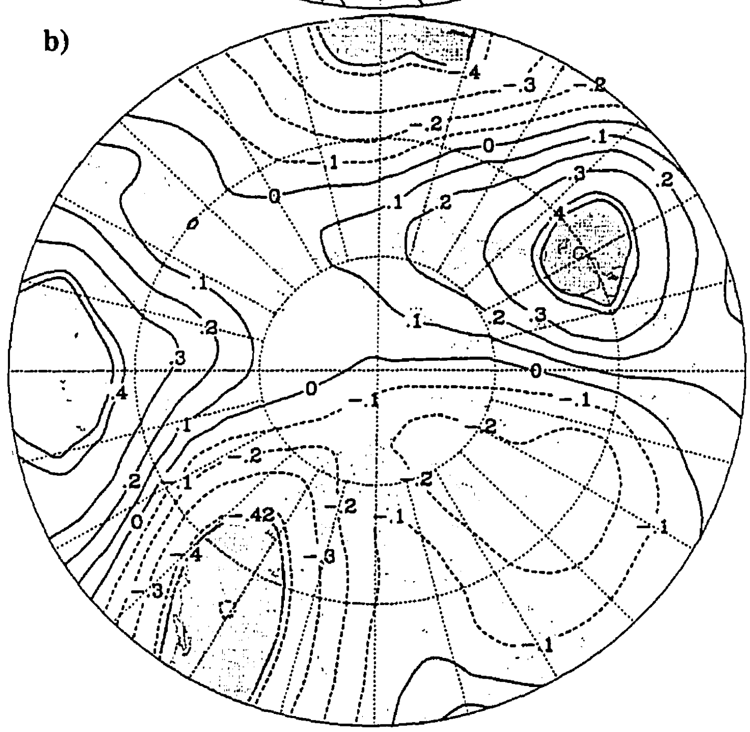

Figure 5.7 As in Figure 5.1, but for a) winter SLP, b) winter 500 Z, and c) 850 T at lag +4.

c)

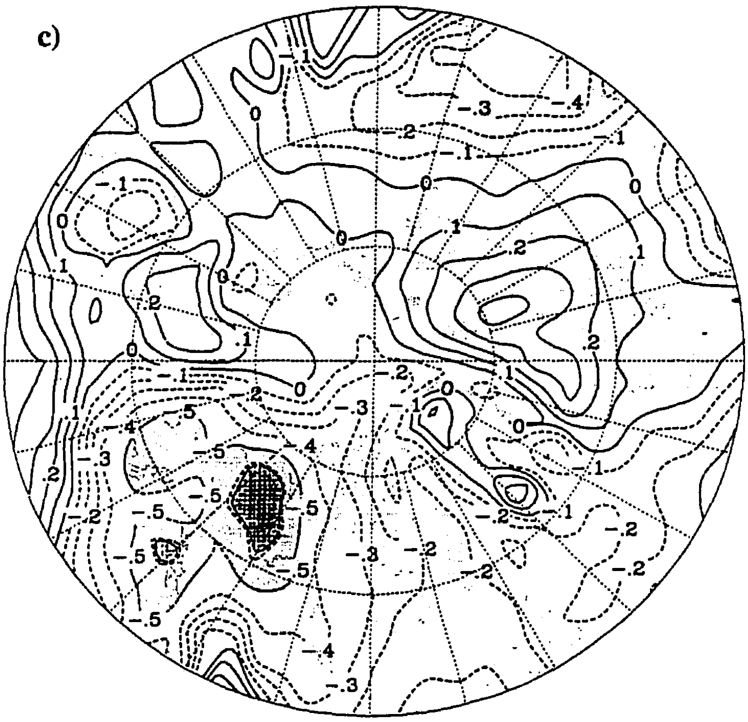

Figure 5.7 cont'd.

IMAGE EVALUATION TEST TARGET (QA-3)

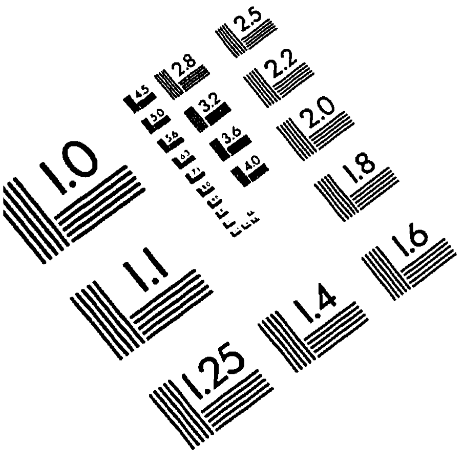

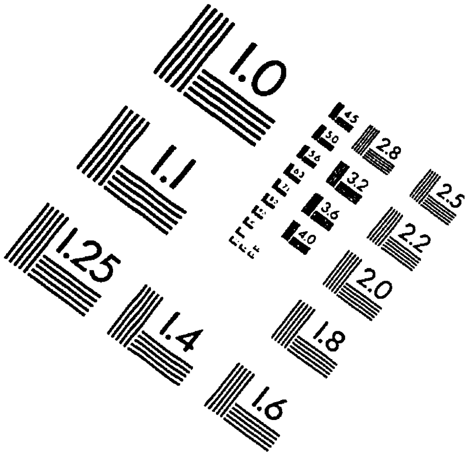

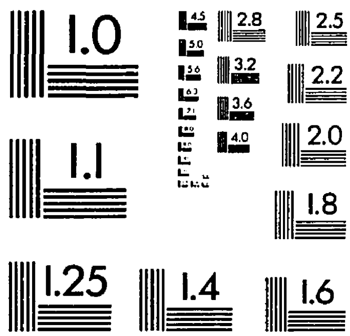

150mm

6″

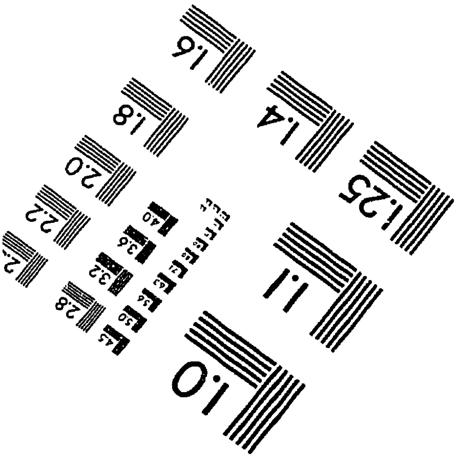

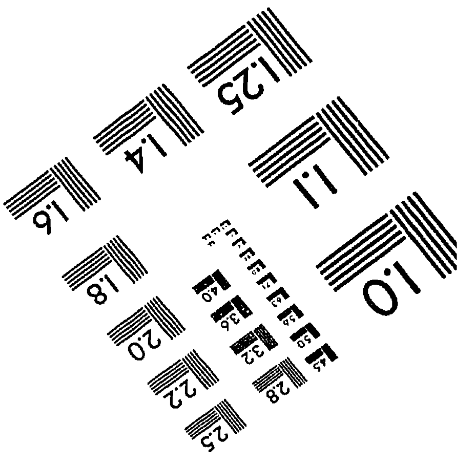

APPLIED IMAGE, Inc
1653 East Main Street
Rochester, NY 14609 USA
Phone: 716/482-0300
Fax: 716/288-5989